https://doi.org/10.1016/j.ymssp.2021.107940

Spectral Based Pipeline Leak Detection Using a Single Spatial Measurement

ALIREZA KERAMAT, Research Assistant Professor[1]
HUAN-FENG DUAN, Associate Professor[2]

[1]Dept. of Civil and Environmental Engineering, The Hong Kong Polytechnic University (HKPolyU), Hong Kong SAR, China. (corresponding author). ORCID: https://orcid.org/0000-0002-6280-4931. Email: keramat.alireza@gmail.com

[2]Dept. of Civil and Environmental Engineering, The Hong Kong Polytechnic University (HKPolyU), Hong Kong SAR, China. ORCID: http://orcid.org/0000-0002-9200-904X. Email: hf.duan@polyu.edu.hk

ABSTRACT

This study offers a vast improvement to the established Matched Field Processing (MFP) method for leak identification in terms of its versatility to pinpoint leaks with a single spatial measurement. All the previous schemes require at least two measurement signals of pressure head as well as transient signal of the upstream flow rate so as to render a solution to the leak identification problem. This study reformulates the one-dimensional identification procedure so that localization can be accomplished using a single spatial measurement. The numerical results convincingly demonstrate that the new method outweighs the conventional one as it provides a smoother objective function and hence robust to identify leaks using observations of greater noise levels. Checked against two recent laboratory experiments, the proposed method gave satisfactory localization to both of which. The new scheme can provide an improved (both in terms of efficiency and accuracy) initial estimate to the multidimensional optimizations required to localize multiple leaks.

Keywords: Leak detection; Water hammer; Signal Processing; Maximum Likelihood Estimation; Matched Field Processing.

1. Introduction

Leak identification in water supply pipelines receives a great deal of attention in order to maintain water resources, downgrade economic losses and prevent water quality impairment [1-3]. The generation of transient waves, and then collecting and processing the system responses have now been established as an efficient and promising technique to determine leak sizes and locations [4]. The transient-based defect detection methods (TBDDM) essentially incorporate a transient solver and collected signals – either in time or frequency domains – in order to seek some system parameters i.e. leaks herein. The primary focus of the present research is on the measurements in that leaks can be identified using only a single spatial transient signal.

In view of the literature of TBDDM developed to date, the so-called inverse transient analysis which sets the transient model against the collected data in the time domain [5-13], and the frequency response function (FRF) approach which adopts simulated and measured frequency spectra [14-28], have been vastly elaborated. Between the two groups, the FRF-based methods are far more desirable because the natural frequencies of a system reveal significant properties of the domain. Besides, in the frequency domain, the transient phenomenon is governed by ordinary differential equations whose analytical solutions are readily available. The Transfer Matrix Method (TMM) provides a fruitful tool to model transient spectrum in a pipe system with multiple leaks and forms the fundamental element of the majority of FRF techniques. The simplest one of which

entails fitting modelled FRFs to measurements by adjusting leakage parameters [16]. Other FRF-based approaches are somehow operating on a similar basis e.g. studying resonance peaks pattern [17] or transient damping [22].

A recently-developed robust approach belonging to the FRF category is the Matched-Field Processing (MFP) or its equivalence – as proved in [29] – the Maximum Likelihood Estimation (MLE) which the current study targets to modify. The articles introduced, investigated, promoted and established the MFP method, most of which co-authored by Wang and Ghidaoui [29-35], are now referred in passing. They suggest a linear transient model in terms of the leak sizes which allows to separate search for leak sizes and leak locations. Their clever idea has led to numerous studies on leak detection such as identification of multiple leaks [30], application of various signal processing techniques in wireless communications [31], iterative beamforming and leak number estimation [32], MFP in viscoelastic pipes [33], incorporating prior information [34], and experimental manifestations [35].

This study addresses a drawback in the aforementioned MFP-based methods [29-35] and proposes a new formulation to tackle it. More specifically, they all suffer from the need to settle at least two measurement stations of the pressure head and one additional measurement station near the upstream boundary. This puts a significant drawback relative to other methods such as [5-28], although all these studies search for the leak sizes and locations simultaneously which is not computationally efficient. It should be emphasized that although numerous papers have recently been conducted based on the MFP approach, no remedy has so far been proposed to resolve this drawback so as to enable localization using a single measurement vector. This is the main motive

to conduct this study which can vastly improve the currently-stablished MFP method of leak identification.

The rest of the paper is structured as follows. In the next section, the TMM equations for the transient analysis in a leaky pipeline, which constitute the basis of this study, are presented. Next, the proposed leak identification approach is formulated which is then followed by numerical results, experimental case studies, discussions and concluding remarks.

2. Transfer matrix approach to transient analysis

The mathematical model of transient waves is delineated and then a linearized representation of the model in terms of leak size is provided. This section provides the fundamental theories of the pressure wave propagation which allows for adapting the established signal processing techniques in the next section.

The mathematical and corresponding leak identification model is illustrated for the pipe system depicted in Fig. 1. Continuity and momentum equations govern the wave propagation in the fluid-filled pipeline. In the Laplace domain with variable $s = \mathrm{i}\omega$, where ω is angular frequency and $\mathrm{i} = \sqrt{-1}$, they can be written in the following matrix representation [36-37]

$$s\mathbf{A}\mathbf{Y} + \mathbf{B}\frac{\partial \mathbf{Y}}{\partial z} = \mathbf{0}, \quad \mathbf{A} = \begin{bmatrix} \frac{1}{A} + \frac{f q_0 \mathrm{sign}(q)}{A^2 D s} & 0 \\ 0 & \frac{g}{a^2} \end{bmatrix}, \quad \mathbf{B} = \begin{bmatrix} 0 & g \\ 1 & 0 \end{bmatrix}, \quad \mathbf{Y} = [q\,, h]^{\mathrm{T}}, \tag{1}$$

where the flow rate q and pressure head h constitute the unknowns of the model and the independent variables are Darcy-Weisbach friction factor f, gravitational acceleration g, inner diameter of pipe D, cross-sectional area of flow A, steady-state flow rate q_0, and longitudinal

direction of the pipe wall z. The formula of the pressure wave speed a in elastic and viscoelastic pipes is different. For elastic pipes

$$a = a_E = \left(\frac{\rho_f}{K} + \frac{\rho_f D}{eE}(1-\nu^2)\right)^{-\frac{1}{2}} \tag{2}$$

in which ρ_f is fluid density, K is bulk modulus, ν is Poisson's ratio, e is pipe-wall thickness, and E is elastic modulus. In the case of a viscoelastic pipe, creep coefficients comprising compliances J_k and retardation times $\tau_k, k = 1, \dots, N_{KV}$ are adopted instead of the elastic modulus, so that the wave speed is estimated through [38-44]

$$a = a_{VE} = \left(\frac{\rho_f}{K} + \frac{\rho_f D}{e}[KV](1-\nu^2)\right)^{-\frac{1}{2}}, [KV] = J_0 + \sum_{k=1}^{N_{KV}} \left(\frac{J_k}{1+s\tau_k}\right) \tag{3}$$

which corresponds to the wave speed in a material governed by generalized Kelvin-Voigt model made from N_{KV} elements and one spring of stiffness J_0^{-1} connect to them in series. In buried pipelines, the surrounding soil may cause the pipe to manifest a viscoelastic attitude so that the pipe and its surrounding soil are advised to be treated as a unified viscoelastic material [44].

Equation (1) offers a system of first order partial differential equations whose analytical solutions are available in the frequency domain given the corresponding initial and boundary conditions [43]. Let indices 1 and 2 denote the two boundaries of a domain (e.g. upstream and downstream) in which the solution to Eq. (1) is sought. By means of the transfer matrix approach, for the state variable $\mathbf{Y}$, the following transfer relation between the two arbitrary points 1 and 2 distanced z_d from each other holds

$$\mathbf{Y}_2 = \mathbf{M}^{NL}_{z=z_d}\mathbf{Y}_1, \quad \mathbf{M}^{NL}_{z=z_d} = \mathbf{S}\,\mathbf{E}_{z=z_d}\,\mathbf{S^{-1}}, \tag{4}$$

in which the superscript "*NL*" indicates that no leak exists between 1 and 2, and matrices **S** and **E** are

$$\mathbf{S} = [\mathbf{a}_1 \quad \mathbf{a}_2], \quad \mathbf{E} = \begin{bmatrix} e^{\frac{-sz}{\lambda_1}} & 0 \\ 0 & e^{\frac{-sz}{\lambda_2}} \end{bmatrix} \tag{5}$$

where the column vectors $\mathbf{a}_i$ and the parameter $\lambda_i, i = 1,2$ are respectively the eigenvectors and eigenvalues of the matrix $\mathbf{A^{-1}B}$, and z is the axial coordinate. Detailed derivation of matrices **S** and **E** is provided in [43]. Calculation of the eigenvalues and eigenvectors in Eq. (5) and substitution of the resulting expressions in Eq. (4) gives the transfer matrix [26, 43]

$$\mathbf{M}_{z_d}^{\mathrm{NL}} = \mathbf{S}\,\mathbf{E}_{z=z_d}\mathbf{S}^{-1} = \begin{pmatrix} \cosh(\mu z_d) & -\frac{1}{\vartheta}\sinh(\mu z_d) \\ -\vartheta\sinh(\mu z_d) & \cosh(\mu z_d) \end{pmatrix}, \quad \vartheta = \frac{\mu\, a^2}{sgA}, \mu = \frac{s}{a}\sqrt{1 + \frac{f q_0 \mathrm{sign}(q)}{ADs}} \tag{6}$$

Now consider transient data of N_s measurement stations located at $z_m, m = 1,2,\dots,N_s$ in a pipeline with a leak having coordinate z_L, in which $z_U < z_L < z_m$. Let α_L (subscript L stands for the leak) denote the characteristic size of each leak which is determined by steady state leakage flow rate Q_n^0, its pressure head H_n^0 and elevation y_n. In the pipe regions between the boundaries and the leak i.e. $z \in [z_U, z_L) \cup (z_L, z_m]$ the field matrix is given by Eq. (1). The flow rate immediately after the leak node is determined by subtracting the leakage discharge from the flow rate before the leak. Accordingly, in case of a single leak, the transfer matrix between the upstream state vector and that of the measurement station whose coordinate is indicated by subscript *m* yields [26, 29, 37]

$$\mathbf{Y}_m = \mathbf{T}\,\mathbf{Y}_U,\ \mathbf{T} = \mathbf{M}_{z_m - z_L}^{NL} \begin{bmatrix} 1 & \alpha_L \\ 0 & 1 \end{bmatrix} \mathbf{M}_{z_L - z_U}^{NL}, \quad \alpha_L = -\frac{Q_L^0}{2(H_L^0 - y_L)} \tag{7}$$

The transfer matrix presented in Eq. (7) can be simplified to (see Appendix A)

$$\mathbf{T} = \mathbf{M}^{NL}_{z_m - z_U} + \alpha_L \mathbf{M}^{SL}_{z_L}, \quad \mathbf{M}^{SL}_{z_L} = \mathbf{M}^{NL}_{z_m - z_L}\, \mathbf{L}\, \mathbf{M}^{NL}_{z_L - z_U}, \quad \mathbf{L} = \begin{bmatrix} 0 & 1 \\ 0 & 0 \end{bmatrix}, \tag{8}$$

where $\mathbf{M}^{NL}_{z_m - z_U}$ is given by Eq. (6) if substituted $z_d = z_m - z_U$, and $\mathbf{M}^{SL}_{z_L}$ is calculated as follows

$$\begin{aligned} \mathbf{M}^{SL}_{z_L} &= \mathbf{M}^{NL}_{z_m - z_L}\, \mathbf{L}\, \mathbf{M}^{NL}_{z_L - z_U} \\ &= \begin{pmatrix} -\vartheta \cosh(\mu z_{Lm}) \sinh(\mu z_{UL}) & \cosh(\mu z_{Lm}) \cosh(\mu z_{UL}) \\ \vartheta^2 \sinh(\mu z_{Lm}) \sinh(\mu z_{UL}) & -\vartheta \cosh(\mu z_{UL}) \sinh(\mu z_{Lm}) \end{pmatrix}, \\ \vartheta &= \frac{\mu\, a^2}{sgA}, \mu = \frac{s}{a} \sqrt{1 + \frac{f q_0 \mathrm{sign}(q)}{ADs}}, \qquad z_{UL} = z_L - z_U, \\ z_{Lm} &= z_m - z_L, \qquad s = \mathrm{i}\omega \end{aligned} \tag{9}$$

Consequently, the state vector at the downstream boundary is related to that at the upstream via

$$\mathbf{Y}_D = \left(\mathbf{M}^{NL}_{z_m - z_U} + \alpha_L \mathbf{M}^{SL}_{z_L}\right) \mathbf{Y}_U \tag{10}$$

Apart from the governing Eqs. (1) which led to Eq. (10), knowledge of the boundary conditions (at the upstream and downstream) is inevitable in order to carry out the transient analysis. Let the data $h_U = h^*$ and $q_D = q^*$ hold respectively as the upstream and downstream boundaries. The application of these boundary values in Eq. (10) sets the following equations at each frequency which are solved simultaneously to arrive at the spectra of unknown boundary variables q_U and h_D:

$$q^* = (m^{NL}_{11} q_U + m^{NL}_{12} h^*) + \alpha_L\, (m^{SL}_{11} q_U + m^{SL}_{12} h^*) \tag{11}$$

$$h_D = (m^{NL}_{21} q_U + m^{NL}_{22} h^*) + \alpha_L\, (m^{SL}_{21} q_U + m^{SL}_{22} h^*) \tag{12}$$

where $m_{ij}, i, j = 1,2$, are elements of the field matrices without leak (indicated by superscript NL) or with a single leak (superscript SL); they are functions of the angular frequency ω. Note that in the forward problem, the leak size characterized by α_L and the leak location z_L (m^{SL}_{12} and m^{SL}_{22} terms are quantified by the leak location) which are system properties have to be known so as to enable

computing h_D and q_U. In the inverse problem, use is made of the transient data collected at least at one location (e.g. either of h_D or q_U) to identify the system properties i.e. leaks herein.

3. Leak localization and size estimation

The leak identification procedure consists of conducting water hammer tests and collecting transient data at some measurement stations. In the MFP-based leak identification method developed by Wang and Ghidaoui [29-35], the transient data of the flow rate at the upstream is necessary. To this end, they proposed to measure the transient pressure head at a node near the upstream boundary so as to compute the flow rate spectrum. Although the main novelty of the current research is to obviate this necessity, for the sake of comparison, the conventional scheme developed in [29] is firstly achieved using a different procedure and then the new approach which just needs a single measurement signal is delineated.

Measurements are inevitably contaminated with noise which usually consists of a zero-mean random quantity. The flow rate spectrum at the upstream can be described as

$$\mathbf{q}_U^M = \mathbf{q}_U + \mathbf{n}_q, \qquad \mathbf{q}_U = \left(q_{U,1}, q_{U,2}, \dots, q_{U,J}\right)^{\mathrm{T}}, \quad \mathbf{n}_q = \left(n_{q,1}, n_{q,2}, \dots, n_{q,J}\right)^{\mathrm{T}} \tag{13}$$

where $\mathbf{q}_U^M$ denotes the measured noisy data, $\mathbf{q}_U$ represents the corresponding noise-free quantities which are in fact the outputs of the transient model and $\mathbf{n}_q$ is a Gaussian white noise with zero mean. Likewise, the pressure head signal collected at *m*-th measurement station can be presented as

$$\mathbf{h}_m^M = \mathbf{h}_m + \mathbf{n}_m, \quad \mathbf{h}_m = \left(h_{m,1}, h_{m,2}, \dots, h_{m,J}\right)^{\mathrm{T}}, \quad \mathbf{n}_m = \left(n_{m,1}, n_{m,2}, \dots, n_{m,J}\right)^{\mathrm{T}}, \quad m = 1,2, \dots, N_s \tag{14}$$

in which N_s is total number of measurement stations. Since the N_s signals are all employed for localization, they can be combined into one long measurement vector $\mathbf{h}^M$ and computed signal $\mathbf{h}$ as follows

$$\mathbf{h}^M = \left(\mathbf{h}_1^M; \mathbf{h}_2^M; \dots; \mathbf{h}_{N_s}^M\right) \ , \qquad \mathbf{h} = \left(\mathbf{h}_1 ; \mathbf{h}_2 ; \dots; \mathbf{h}_{N_s}\right) \ , \tag{15}$$

To calculate the pressure head at the *m*-th measurement station, the following equation similar to Eq. (12) holds

$$\begin{aligned} h_m = (m_{21}^{NL} q_U + m_{22}^{NL} h^*) + \alpha_L \, (m_{21}^{SL} q_U + m_{22}^{SL} h^*), \qquad m_{21}^{NL} = -\vartheta \sinh(\mu z_d) \, , \\ m_{22}^{NL} = \cosh(\mu z_d) \, , \qquad m_{21}^{SL} = \vartheta^2 \sinh(\mu z_{Lm}) \sinh(\mu z_{UL}) \, , \\ m_{22}^{SL} = -\vartheta \cosh(\mu z_{UL}) \sinh(\mu z_{Lm}) \, , \qquad z_d = z_m - z_U, \\ z_{Lm} = z_m - z_L, \qquad z_{UL} = z_L - z_U \end{aligned} \tag{16}$$

Note that Eq. (16) provides the pressure head magnitude corresponding to each frequency.

If the measured data are statistically independent with the same standard deviation, then the likelihood of the true modelled signal is the product of the likelihood of each entry of measurement vector. Maximizing this likelihood corresponds to minimizing the square error between measured and calculated pressures which provides the best fit parameters [45], so

$$\{\hat{z}_L, \hat{\alpha}_L\} = \ \arg\min_{z_L, \alpha_L} \|\mathbf{h}^M - \mathbf{h}\|^2, \tag{17}$$

In this study, a constant pressure head at the upstream is assumed whereas a delta function (impulse) generates transient waves at the downstream, hence

$$h^*_{z=z_U} = 0, \ q^*_{z=z_D} = 1 \tag{18}$$

The general approach of the estimation procedure is based on the transient model with one leak. The reasons for exploiting such a model are: (i) in case of more than one leak, the results of the one-leak based model provide a satisfactory initial guess; (ii) such a method (with one leak) can

localize two leaks in many cases; (iii) the optimization process is extremely simplified because the domain can be enumerated; (iv) identification based on multiple-leaks model in real practice especially in the presence of measurement noise is difficult and less reliable. The application of the one-leak transient model allows to enumerate the domain and estimate the value of the cost function defined in Eq. (17). Note that the one-dimensional approaches for leak identification can be extended to exploit multiple-leak models, but in turn the localization leads to a complex optimization procedure which is extremely no-convex and cumbersome to find its global extremum.

Because there are multitude of MFP-based studies requiring upstream measurement of flow rate, firstly, such a model is presented. Then it is demonstrated that the upstream flow rate can be estimated using the system properties thus leading to a localization scheme that requires only a single measurement signal.

3.1. Old method: available measurement of transient upstream flow rate

This section mainly seeks to revisit the recently established MFP for leak identification [29-35]. It assists making inference about the novelty that this study introduces to the classical approach.

Considering Eq. (16) and the boundary conditions in Eq. (18), the pressure head at the measurement station which give rise to the vector $\mathbf{h}$ defined in Eq. (15) is obtained. By substituting the result in Eq. (17) it yields

$$\{\hat{z}_L, \hat{\alpha}_L\} = \arg\min_{z_L,\alpha_L} \sum_{j=1}^{J}\sum_{m=1}^{N_s} \Big(h_m^M(\omega_j) - \Big(m_{21}^{NLm}(\omega_j) q_U^M(\omega_j) + \alpha_L m_{21}^{SLm}(\omega_j) q_U^M(\omega_j) \Big) \Big)^2$$

$$= \arg\min_{z_L,\alpha_L} \sum_{j=1}^{J}\sum_{m=1}^{N_s} \Big(h_m^M(\omega_j) - h^{NLm}(\omega_j) - \alpha_L G^m(\omega_j) \Big)^2 \tag{19}$$

$$= \arg\min_{z_L,\alpha_L} \sum_{k=1}^{N_s J} \big(\Delta h(\omega_k) - \alpha_L G(\omega_k) \big)^2 := \arg\min_{z_L,\alpha_L} \|\Delta\mathbf{h} - \alpha_L \mathbf{G}\|^2 ,$$

$$m_{21}^{NLm} = m_{21}^{NL}(z = z_m), \qquad m_{21}^{SLm} = m_{21}^{SL}(z = z_m),$$

$$m = 1,2,\dots,N_s, \qquad k = 1,2,\dots,J, J+1,\dots,2J,\dots,N_s J$$

An inspection of the definitions of $\Delta\mathbf{h}$ and $\mathbf{G}$ in Eq. (19) reveals that the former is devoid of the leak size and location and the latter is only a function of the leak location. Consequently, for any leak location, the size of the leak offers a single variable optimization problem whose solution yields

$$\hat{\alpha}_L = \frac{\mathbf{G}^H \Delta\mathbf{h}}{\mathbf{G}^H \mathbf{G}}, \qquad G_k = m_{21}^{SL}(\omega_k) q_U^M(\omega_k), \tag{20}$$

$$\Delta h_k = h_k^M(\omega_k) - m_{21}^{NL}(\omega_k) q_U^M(\omega_k)$$

Substituting back the estimated leak size into the last expression of Eq. (19) yields

$$\{\hat{z}_L\} = \arg\min_{z_L,\alpha_L} \|\Delta\mathbf{h} - \alpha_L \mathbf{G}\|^2$$

$$= \arg\min_{z_L} \left\| \Delta\mathbf{h} - \frac{\mathbf{G}\mathbf{G}^H}{\mathbf{G}^H\mathbf{G}} \Delta\mathbf{h} \right\|^2 = \arg\max_{z_L} \left(\Delta\mathbf{h} \frac{\mathbf{G}\,\mathbf{G}^H}{\mathbf{G}^H\mathbf{G}} \Delta\mathbf{h} \right) \tag{21}$$

$$:= \arg\max_{z_L} (B^2)$$

The resulting objective function in Eq. (21) is equivalent to that presented by Wang and Ghidaoui [29-35]. The last equality holds due to the fact that the expression in the parenthesis is always a positive scalar quantity indicated by B^2 hereafter.

3.2. New method: unavailable measurement of upstream transient discharge, localization using a single spatial measurement

The idea is that according to Eqs. (11) and (12), if system properties, specifically leaks herein, are known, then both upstream flow rate and downstream pressure head can be calculated. In the parameter estimation problem though, the pressure head at any measurement station can be formulated in terms of the unknown parameters. Hence the objective function as a function of only unknown system properties is achievable.

In the case that the measurement of the flow rate at the upstream is not carried out, Eq. (11) can be used to calculate the flow rate in terms of the leak characteristics. Considering Eq. (11) along with the boundary conditions defined in Eq. (18), the flow rate at the upstream is found as

$$q_U = \frac{1}{m_{11}^{NLD} + \alpha_L m_{11}^{SLD}}, m_{11}^{NLD} = m_{11}^{NL}(z = z_D), m_{11}^{SLD} = m_{11}^{SL}(z = z_D) \tag{22}$$

Substituting q_U from Eq. (22) in Eq. (16) in conjunction with the boundary conditions in Eq. (18) allows to compute the pressure head at the measurement stations independent from the upstream flow rate:

$$h_m = (m_{21}^{NL} + \alpha_L m_{21}^{SL})\, q_U = \frac{m_{21}^{NLm} + \alpha_L m_{21}^{SLm}}{m_{11}^{NLD} + \alpha_L m_{11}^{SLD}}, \qquad m_{21}^{NLm} = m_{21}^{NL}(z = z_m), \tag{23}$$
$$m_{21}^{SLm} = m_{21}^{SL}(z = z_m), \qquad m = 1,2, \dots, N_s$$

Hence, the estimation in Eq. (17) reduces to

$$\{\hat{z}_L, \hat{\alpha}_L\} = \arg\min_{z_L,\alpha_L} \sum_{j=1}^{J}\sum_{m=1}^{N_s}\left(h_m^M(\omega_j) - \frac{m_{21}^{NLm}(\omega_j) + \alpha_L m_{21}^{SLm}(\omega_j)}{m_{11}^{NLD}(\omega_j) + \alpha_L m_{11}^{SLD}(\omega_j)}\right)^2 =$$

$$= \arg\min_{z_L,\alpha_L} \sum_{j=1}^{J}\sum_{m=1}^{N_s}\left(\frac{h_m^M(\omega_j)m_{11}^{NLD}(\omega_j) - m_{21}^{NLm}(\omega_j) + \alpha_L\left(m_{11}^{SLD}(\omega_j)h_m^M(\omega_j) - m_{21}^{SLm}(\omega_j)\right)}{m_{11}^{NLD}(\omega_j) + \alpha_L m_{11}^{SLD}(\omega_j)}\right)^2 \quad (24)$$

The least square solution to the optimization problem presented in Eq. (24) is achieved when the numerator becomes zero, hence

$$\alpha_L\,\mathbf{G} = \Delta\mathbf{h}, \qquad G_k = m_{21}^{SL}(\omega_k) - m_{11}^{SLD}(\omega_k)h_k^M(\omega_k),$$
$$\Delta h_k = h_k^M(\omega_k)m_{11}^{NLD}(\omega_k) - m_{21}^{NL}(\omega_k), \quad (25)$$
$$k = 1,2,\dots,J,J+1,\dots,2J,\dots,N_s J$$

Like the previous method, $\Delta\mathbf{h}$ is independent from leak properties and $\mathbf{G}$ is a function of leak locations and not leak sizes. The leak size is the solution of Eq. (25) which is

$$\hat{\alpha}_L = \frac{\mathbf{G}^H\Delta\mathbf{h}}{\mathbf{G}^H\mathbf{G}}, \qquad G_k = m_{21}^{SL}(\omega_k) - m_{11}^{SLD}(\omega_k)h_k^M(\omega_k),$$
$$\Delta h_k = h_k^M(\omega_k)\, m_{11}^{NLD}(\omega_k) - m_{21}^{NL}(\omega_k) \quad (26)$$

Substituting back the estimated leak size into Eq. (24) leads to a similar objective function with different definitions for $\Delta\mathbf{h}$ and $\mathbf{G}$:

$$\{\hat{z}_L\} = \arg\min_{z_L,\alpha_L} \sum_{k=1}^{N_s J}\left(\frac{\Delta h_k + \alpha_L G_k}{m_{11}^{NLD}(\omega_k) + \alpha_L m_{11}^{SLD}(\omega_k)}\right)^2 \approx \arg\min_{z_L,\alpha_L}\|\Delta\mathbf{h} - \alpha_L\,\mathbf{G}\|^2$$
$$= \arg\min_{z_L}\left\|\Delta\mathbf{h} - \frac{\mathbf{G}\mathbf{G}^H}{\mathbf{G}^H\mathbf{G}}\Delta\mathbf{h}\right\|^2 = \arg\max_{z_L}\left(\Delta\mathbf{h}\,\frac{\mathbf{G}\,\mathbf{G}^H}{\mathbf{G}^H\mathbf{G}}\Delta\mathbf{h}\right) \coloneqq \arg\max_{z_L}(B^2) \quad (27)$$

Note that the third expression is achieved on account of the fact that $m_{11}^{SLD} \ll m_{21}^{SL}$ which in turn justifies to neglect $\alpha_L m_{11}^{SLD}$ in comparison to $\alpha_L G_k$. The inequality will be closely investigated in

the next section. The location of the leak (z_L) can by realized by plotting B^2 against all domain nodes (search space) and identifying the place of global maximum on the graph. Once the leak location is determined, the leak size can be estimated via Eq. (26).

4. Numerical Results and Discussion

This section serves as numerical examples of single and multiple leaks localization using the described two schemes. The properties of each method, their strengths and weaknesses and corresponding error analysis for each one are discussed.

4.1. Preliminaries

A typical reservoir-pipe-valve system with one (two) leak(s) is considered for localization using the two methods. The system specifications are: pipe length $L = 2000$ m, inner diameter of pipe $D = 0.5$ m, bulk modulus of fluid $K = 2.1$ GPa, elastic modulus and thickness of the pipe wall $E = 210$ GPa, $e = 1$ cm , upstream reservoir head $h_R = 25$ m, outflow rate from reservoir (before the leak) $Q^0 = 15.3\ \mathrm{Ls}^{-1}$, leakage flow rate $Q_L^0 = 3\ \mathrm{Ls}^{-1}$, fluid's density $\rho_f = 1000\ \mathrm{kg\,m}^{-3}$, friction factor of pipe $f = 0.02$. The wave speed is computed as $a_E = 1200\ \mathrm{ms}^{-1}$. The measured pressures at the downstream boundary, $z_D = 2000$ m, as well as at $z = 1800$ m (used only for the old method), both indicated by the superscript *M* in the preceding formulation, are used in the leak identification. All measurements of pressure and flow rate are assumed to follow the Gaussian distribution so they are first computed using Eqs. (11) and (12), and then they are added to a **0**-mean normal white noise to make the hypothetical noisy data of each element of measurement. The noise level is defined based on the signal to noise ratio (SNR) which herein is quantified by

$$\mathrm{SNR} = 20\log_{10}\left(\frac{\|\mathbf{h}-\mathbf{h}^{\mathrm{NL0}}\|}{\sigma\sqrt{N_s J}}\right) \tag{28}$$

in which the scalar quantity $\|\mathbf{h}-\mathbf{h}^{\mathrm{NL0}}\|$ represents the norm of differences between spectra of head with leak ($\mathbf{h}$) and without leak ($\mathbf{h}^{\mathrm{NL0}}$), and σ stands for the standard deviation of the Gaussian white noise. One should notice to the difference between $\mathbf{h}^{\mathrm{NL}}$ and $\mathbf{h}^{\mathrm{NL0}}$: the first one is obtained based on $\mathbf{q}_U$ which itself is obtained for the leaky system considering Eqs. (11), (12) and (18) (to identify the definition of $\mathbf{h}^{\mathrm{NL}}$ see Eq. (19)), but the latter corresponds to the transient solution in which the leak size is set to zero or in other words, it is given based on $\mathbf{q}_U^0$ which itself is determined for a system without leak (superscript 0 on flow rate denotes no-leak transient data). In this view, the definition of SNR in the current research differs from that of [29-35], since all these studies need $\mathbf{q}_U$ to be known i.e. they inevitably apply $\mathbf{h}^{\mathrm{NL}}$.

The frequencies up to $n_{\max}\omega_{th}$, in which ω_{th} is the fundamental water hammer frequency of the (pipe and contained fluid) system, are adopted for localization, hence in the case that resonant and anti-resonant frequencies are used the bandwidth is $\omega = \{n\omega_{th} : n = 1,2,\dots,n_{\max}\}$.

4.2. Localization of a single leak

The described pipe system has one leak of effective size $A_L = 135.4\ \mathrm{mm}^2$ and characteristic size $\alpha_L = -\frac{0.5\ Q_L^0}{(H_L^0 - y_L)} = -60\ \mathrm{mm}^2\mathrm{s}^{-1}$ located at $z_L = 400$ m from the upstream reservoir. The flow rate and pressure head at the leak node are $Q_L^0 = 3\ \mathrm{Ls}^{-1}$ and $H_L^0 = 24.98$ m, respectively. The aim is to compare the results of the two methods by plotting their objective functions pointed out in Eq. (21) and Eq. (27) corresponding to the old and the proposed method, respectively. The hypothetical measurement signals are generated using Eqs. (13)-(16), in which for the forward analysis, the

actual location of the leak is imposed in Eq. (16) to generate the transient data. The boundary conditions presented in Eq. (18) are applied and the first 16 resonant peaks i.e. $\omega = \{n\omega_{th} : n = 1,3,\dots,31\}$ in which $\omega_{th} = a\pi(2L)^{-1} = 0.94\,\text{rad.}\,\text{s}^{-1}$ is the fundamental water hammer frequency, are adopted to pinpoint the leak. Appendix B provides the results obtained by Eq. (16) before they are contaminated by the white noise.

4.2.1 Typical results of each method

The objective functions are enumerated for all nodes of the domain i.e. $z \in (0, L)$, and the output corresponding to each method are depicted in Fig. 2. In the figure, the dashed line represents the actual leak location and the ellipses stand for the locations of the measurement stations. The exercise has been carried out using noise-free data and the minimum number of sensors required to deploy i.e. three for method 1 and one for method 2. A comparison of the two graphs in Fig. 2 reveals that both merit functions show their maximum at the actual leak hence they can correctly pinpoint the leak. However, the new method outweighs the first one as it suppresses the side lobes to a greater extent, a property which is of particular significance when the noise level is high or the number of leaks are a priori unknown which both usually hold in real practice.

4.2.2 Performance in a noisy environment

When noise is present in an identification procedure, statistical properties provide a worthwhile measure to assess the method. To this end, the leak detection process is repeated for several observations, and then the desired statistical properties are estimated from the identification results. Localization of leaks which are bigger in size (α_L is relatively high) is easier than small leaks, because they produce larger transient reflections quantified by $\|\mathbf{h} - \mathbf{h}^{\text{NL0}}\|$. Likewise, leak

detection using measurements of low noise level (small σ) is more accurate. That is why usually the ratio of these two defined by SNR in Eq. (28) is studied to quantify the estimation error.

The noisy signals as presented in Eqs. (13)-(15) are hypothetically generated, in which the standard deviation σ of the noise vector **n** is defined based on SNR presented in Eq. (28). The noisy signals are used for leak detection using the two methods for various SNR values. Because leak-location identification is more the issue of concern, the error of localization (being $|\hat{z}_L - z_L|$ in which z_L, $\hat{z}_L$ are actual and estimated 1ocations respectively) is estimated from the results of each simulation. The generation of the measurement signal and the identification using each method is repeated for 50 times and the mean and 95% confidence interval corresponding to each method and noise level are presented in Fig.3. The graphs clearly demonstrate that the new method is extremely more robust than the old method as it can pinpoint leaks in quite higher noise levels.

An intuitive perception on the performance of the two methods subject to random measurements can be provided. The uncertainty of the localization may be realized by inspecting the random vectors $\mathbf{G}, \Delta\mathbf{h}$ employed in the objective functions of each method; see Eq. (20) for the old method and Eq. (26) for the new method. Note that for any constant c and random variable X, this property of variance (Var) holds: $\mathrm{Var}(cX) = c^2\mathrm{Var}(X)$. In view of Eq. (20), the variance of each entry of the vectors **G** and $\Delta\mathbf{h}$ is related to the variance of measurements via

$$\mathrm{Var}(G_k) = (m_{21}^{SL})^2\,\mathrm{Var}(q_{U,k}^M) = (m_{21}^{SL})^2\sigma^2,$$
$$\mathrm{Var}(\Delta h_k) = \mathrm{Var}(h_k^M) - (m_{21}^{NL})^2\mathrm{Var}(q_{U,k}^M) = \sigma^2 + (m_{21}^{NL})^2\sigma^2, \tag{29}$$

in which σ^2 denotes the variance of each element of measurement vectors and the second equality holds because h_k^M and $m_{21}^{NL}q_U^M$ are statistically independent. Likewise, for the new method, Eq. (26) allows for

$$\mathrm{Var}(G_k) = (m_{11}^{SLD})^2\,\mathrm{Var}(h_k^M) = (m_{11}^{SLD})^2\sigma^2,$$
$$\mathrm{Var}(\Delta h_k) = (m_{11}^{NLD})^2\mathrm{Var}(h_k^M) = (m_{11}^{NLD})^2\sigma^2, \quad (30)$$

The variability of the two vectors $\mathbf{G}, \Delta\mathbf{h}$ gives rise to the uncertainty in the merit functions which in turn leads to localization error. Equations (29) and (30) indicate that the values of $m_{11}^{NLD}, m_{21}^{NL}, m_{11}^{SLD}$ and m_{21}^{SL} significantly contribute to the level of uncertainty of the two vectors $\mathbf{G}, \Delta\mathbf{h}$ and hence the merit function they constitute. Figure 4 compares m_{11}^{NL} and m_{21}^{NL} and Fig. 5 depicts the values of m_{11}^{SL} and m_{21}^{SL} for all frequencies at the valve position (downstream) as the measurement station. As seen in Fig.5, since the quantities of m_{11}^{SL} and m_{21}^{SL} depend on the leak position, several locations for the leak is enumerated so as to provide a rough estimate of one against the other. Since m_{21}^{NL} is considerably larger than m_{11}^{NL} (see Fig. 4) and so is for m_{21}^{SL} being larger than m_{11}^{SL} (see Fig. 4), the second method is expected to have smaller variance, thus offering a more stable and robust localization approach which is in accordance with what was presented as the error curves in Fig. 3.

4.3. Localization in case of two leaks

The developed single-leak-based methods can also identify two leaks. Nevertheless, they fail to pinpoint two leaks in some cases [29, 31]. Accordingly, they are not suggested as a robust method of leak identification but on the other hand, the single-leak based models can by far contribute to successful localizations when multi-leak models are employed. More specifically, the results of single-leak based models can be considered as an efficient initial guess for multiple-leak based models which are complicated and computationally expensive but accurate. Methods with multiple leaks lead to multi-dimensional non-convex optimization problems which usually have multitudes of local extremums that make them inefficient. Note that the hypothetical measurement signals

used for localization as presented in Eqs. (13) and (14) are generated using a two-leak transient model and that is the reason for inaccuracy of the single-leak based localization methods in some cases [29, 31].

This section firstly presents some typical outputs of each localization method for a two-leak system and then argues their performance in case they are employed to pinpoint two leaks or to provide initial guess for advanced algorithms. In both investigations, the proposed method seems to overcome the old one.

4.3.1 Typical results

Leak detection in the system with two leaks of size $A_L = 135.4\ \text{mm}^2$ located at $z_1 = 700$ m and $z_2 = 1600$ m from the upstream reservoir is investigated. Since the main flow rate before transients is only $Q^0 = 5\ \text{Ls}^{-1}$, the steady-state friction along the pipeline is too small and negligible, hence the reservoir pressure head of $h_R = 25$ m remains at the leak nodes. In the first attempt, the frequency range $\omega = \{n\omega_{th} : n = 1,2,\dots,31\}$ is employed using the two methods to identify the leaks. Depicted in Fig. 6a, b, both the conventional and the new method are roughly successful in localizing leaks as they both indicate their maximum at or near the actual leak location. The ellipses on the horizontal axis represent the location of measurement stations (hydrophones).

In the other attempt, localization is carried out using frequencies $\omega = \{n\omega_{th} : n = 1,2,\dots,51\}$ and the results of the two methods are plotted in Fig. 7. It is clear from the recent results that the conventional method which requires two measured signals of the pressure head as well as the spectra of the upstream flow rate does not return correct results but the output of the new method is again satisfactory.

The results displayed in Figs. 6 and 7 are extremely sensitive to the location of the leaks. An investigation into this issue is carried out by considering several leak detection exercises consisting of different locations of the first and second leak. The following criterion is defined to estimate the error of the localizations

$$\varepsilon_1 = \min\left((|z_1 - z_1^{\max}| + |z_2 - z_2^{\max}|), (|z_1 - z_2^{\max}| + |z_2 - z_1^{\max}|)\right) \qquad (29)$$

in which z_1 and z_2 represent the locations of the first and second leak and $z_1^{\max}$ and $z_2^{\max}$ respectively indicate the position of first and second local maxima obtained by one of the single-leak based methods (the first local maxima corresponds to the global optimum). The results of the two methods in which the position of the first leak is fixed at $z_1 = 200$ m from the upstream reservoir and the second leak z_2 is moved between 400 m and 1800 m is plotted in Fig. 8a. The estimated error defined based on ε_1 for the other leak positions including $z_1 = 400$ m and $z_2 \in \{600{:}\,200{:}\,1800\}$ (Fig. 6b), $z_1 = 600$ m and $z_2 \in \{800{:}\,200{:}\,1800\}$ (Fig. 6c), $z_1 = 800$ m and $z_2 \in \{1000{:}\,200{:}\,1800\}$ (Fig. 6d), $z_1 = 1000$ m and $z_2 \in \{1200{:}\,200{:}\,1800\}$ (Fig. 6e), $z_1 = 1200$ m and $z_2 \in \{1400{:}\,200{:}\,1800\}$ (Fig. 6f), $z_1 = 1400$ m and $z_2 \in \{1600{:}\,200{:}\,1800\}$ (Fig. 6g) and $z_1 = 1600$ m and $z_2 = 1800$ (Fig. 6h) are displayed in which the continuous line corresponds to the results of the previous method [29] and the dashed line indicate those of the new method. As seen, the estimated error of the two methods is substantial in some leak cases demonstrating that the single-leak based models cannot be suggested as a robust approach for multiple-leak identification. Although the maximum error of the old method is clearly larger, no firm conclusion regarding the priority of one method over the other can be drawn from the results, when they are used to pinpoint two leaks. Nevertheless, the proposed method gets more credit because it only needs a single measurement vector of pressure head. To further compare the two

methods, the estimated errors in each graph which correspond to a fixed location for the first leak and various positions of the second leak are averaged and the result is displayed in Fig. 9. For example in the previous method (continuous line), considering Fig. 8e which corresponds to $z_1 = 1000$ m, the mean error is $(400 + 800 + 0 + 1600)/4 = 700$ m. The comparison between the two methods shown in Fig. 9 reveals that the new method on average outweighs the conventional one, a consequence which was also drawn in view of Figs. 7a, b.

Regarding the error pattern of localization with the position of leaks some points are worthy of noting. If the leaks are too close, then their trace in the objective function are combined together thus leading to a lobe between the two leaks with a wider width [29]. A similar justification can be drawn in the time domain regarding the interaction of traces of close defects [46, 47]. For distant leaks, the localization error mainly varies by the mode shapes of each frequency and that is the reason for error variations with the leaks positions. More specifically, Louati et al. [48] showed that a leak located at an antinode of a given mode will induce a maximum reflection, and hence the corresponding peak amplitude in the spectrum is a minimum. This implies that such a wave can favourably identify that leak. By contrast, if a leak is located at a stagnant point of a given mode, it attributes to a minimum reflection and hence allows for a peak in the spectrum.

The minimum probing wave length corresponds to the wave with highest frequency, so that $\lambda_{\min} = a.2\pi(51\omega_{th})^{-1} = 156.9$ m. The spatial Nyquist criterion states that the resolution limit is equal to half the minimum probing wavelength $0.5.\lambda_{\min} = 78.4$ m, hence the leaks distances considered to be 200 m which is far byond the required condition.

4.3.2 Performance in view of an initial guess for advanced methods

The localization result shown in Fig. 7a indicate that the objective function of the conventional method yields a local maximum at the actual leak position. Although failed in view of localization, such a result is still of great importance when methods based on multiple leaks which lead to multi-dimensional optimizations are incorporated. Because, all the local maxima provided by the current single-leak based methods can be considered as initial search space of the advanced methods thus enabling to generate potential sets of leak candidates. A similar approach is elaborated by Wang et al. [32]. In view of this idea, let the vector $\mathbf{z}^{\max}$ denote the set of all local maxima found by means of a single-leak based method, like those numbered in Figs. 6 and 7. Another criterion for error estimation is defined to compare the performance of the two methods as follows

$$\begin{gathered}\varepsilon_2 = \varepsilon_{L1} + \varepsilon_{L2} = \min\left(\left|\mathbf{z}^{\max} - z_1\mathbf{1}\right|\right) + \min\left(\left|\mathbf{z}^{\max} - z_2\mathbf{1}\right|\right), \\ \mathbf{z}^{\max} = \left(z_1^{\max}, z_2^{\max}, \dots, z_{N_{LM}}^{\max}\right)^{\mathrm{T}}\end{gathered} \tag{30}$$

where N_{LM} represents the number of local maxima and $\mathbf{1}$ stands for a column vector of ones with N_{LM} elements. This error estimation criterion is applied to investigate the performance of each scheme similar to the study carried out for ε_1 defined in Eq. (29). The results of the survey are plotted in Fig. 10a-h in which z_1 is fixed and respectively corresponds to each element of the set $\{200{:}\,200{:}\,1600\}$ and z_2 varies in the region recognized by the horizontal axis of each figure. The average of localization results in each figure of Figs. 10a-h is shown in Fig. 11. This set of results indicate that the two methods behave quite differently and usually lead to distinct solutions when used for two leak cases, yet on average, their performance is analogous.

5. Experimental case studies

To examine the proposed method subject to real localization problems, two well-known laboratory experiments recently carried out in the Water Engineering Laboratory of University of Perugia [9, 33] and the Water Resources Research Laboratory at the Hong Kong University of Science and Technology (HKUST) [33, 35] are investigated. The localization results for these experiments are thoroughly investigated using the old method in [33], hence they are not repeated here. The leak identifications in this section are accomplished using the proposed method which can render the results based on a single spatial measurement.

5.1. Perugia test

The transient waves are generated in a tank-HDPE pipeline-valve system with the specifications provided in Table 1. The creep coefficients of the viscoelastic pipe given in the table have been calibrated based on the collected transient data using the approach explained in [35, 42]. A leak of effective size $68\ \text{mm}^2$ has been located at $z_L = 60.84\ \text{m}$ from the upstream tank in the pipe of length $166.28\ \text{m}$. The full closure of the downstream valve in $T_c = 0.073\ \text{s}$ generates transient waves as depicted in Fig. 12a in the time and Fig. 12b in the frequency domain. Note that theoretically, it is possible to identify a system using the first half period of transients. Nevertheless, the use of a short time span results in a jagged spectrum curve due to the insufficient time for the FFT scheme as discussed in [56]. The procedure to obtain the frequency spectrum from the time data is detailed in [33, 56]. Before embarking on the localization assessment, one should notice that according to the shown pressure head spectrum, for $\omega/\omega_{th} > 20$, the amplitudes are quite noisy, indicating that the shortest reliable probing wavelength is $\lambda_{\min} = 2\pi a/\omega = \pi a/(10\,\omega_{th}) =$

33.2 m. In view of the Nyquist-Shannon sampling theory, half of this quantity is the resolution limit meaning that a method which can resolve the domain beyond this limit is a super-resolution scheme.

The proposed method as well as the previous one can apply the information corresponding to all frequencies (as opposed to other methods which only adopt resonant frequencies e.g. [17, 19]). As a consequence, a fairly fine $\Delta\omega$ is incorporated in localization which allows for the highest possible resolution. The results corresponding to different signal bandwidth of the observed spectrum in Fig. 12b are plotted in Figs. 13a-d. The frequencies used are $\omega = \omega_{th} \times (1{:}\,0.01{:}\,n_{\max})$, the aforementioned resolution limit is $\lambda_1 = 0.5\,\lambda_{\min}$ and the identification error is denoted by $\varepsilon_1 = |\hat{z}_L - z_L|$. The output results of which for (a) $n_{\max} = 8, \lambda_1 = 41.57$ m, is $\varepsilon_1 = 13.16$ m, (b) $n_{\max} = 12, \lambda_1 = 27.71$ m, $\varepsilon_1 = 4.16$ m, (c) $n_{\max} = 16, \lambda_1 = 20.78$ m, $\varepsilon_1 = 2.84$ m, and (d) $n_{\max} = 20, \lambda_1 = 16.63$ m, $\varepsilon_1 = 1.16$ m, as they are respectively shown in Figs. 13a-d. As seen, for all realizations, the estimated error is considerably smaller than the resolution limit implying that the method is robust to convey all available information to pinpoint the leak with great accuracy.

To further assess the identified results, the estimated leak location and size along with the actual ones are applied as inputs to the forward transient model to reconstruct each spectrum and make comparisons with the observations. Measured signal (in continuous black), and the reconstructed spectrum corresponding to the estimated and actual leak (in continuous red and dashed blue, respectively), are plotted in Fig. 14 a-d for the localizations illustrated in Fig. 13a-d, respectively. The simulation results corresponding to the estimated and actual leak are favourably matched, manifesting that the identifications are satisfactory for the given observations. However, the

simulations results (either based on the estimated or the actual leak) get slightly skewed with respect to the measurements. This suggests that a more comprehensive transient model or improved calibrations for viscoelasticity and unsteady friction can enhance the agreement between measurements and simulations and hence increase the accuracy.

Table 1. Pipe and flow specifications of the Perugia experiment [9, 33].

$D = 93.3$ mm	$J_0 = 0.68 \times 10^{-9}\text{Pa}^{-1}$	$\tau_1 = 0.05$ s	$J_1 = 1.061 \times 10^{-10}\text{Pa}^{-1}$
$\tau_2 = 0.5$ s	$J_2 = 1.05 \times 10^{-10}\text{Pa}^{-1}$	$\tau_3 = 1.5$ s	$J_3 = 0.905 \times 10^{-10}\text{Pa}^{-1}$
$e = 7.5$ mm	$\nu = 0.43$	$\rho = 1000$ kg/m^3	$\kappa = 2.1$ GPA
$Q_0 = 4.75$ L/s	$H_T = 18.28$ m	$a = 374.2$ m/s	$Q_{0L} = 1.28$ L/s

5.2. HKUST test

To reconfirm the proposed method for leak detection in real laboratory pipelines, another test is carried out. It belongs to transients and leak identification tests in a 144 m HDPE pipeline with the specifications presented in Table 2. The system is supplied with a pump at the upstream and the full closure of a downstream valve excites the system. The creep coefficients provided in Table 2 are calibrated using the transient data for the leak-free test case, although the approaches of [50-52] for a leaky pipe can also be utilised. The leak is located at $z_L = 45.58$ m, its effective size is $A_L = 10.7$ mm^2 and its discharge ratio to the main pipe flow at steady state is $Q_{0,L}/Q_0 = 0.4$. Only a single spatial measurement vector collected at the valve as depicted in Fig. 15a along with its spectrum in Fig. 15b is incorporated to pinpoint the leak.

The proposed method is applied to identify the leak location using several signal bandwidths in view of Fig. 15b and the appropriate set of frequencies proposed by Wang et al. [33] for the old method. A very fine $\Delta\omega$ is incorporated such that adopting more frequencies do not significantly alter the estimated location. Frequency contents up to $n_{\max}$ harmonics as depicted in Fig. 16a-h are exploited to estimate the leak location. The maximum number of employed resonant frequency $n_{\max} = \omega/\omega_{th}$ and the corresponding resultant error $\varepsilon_1 = |\hat{z}_L - z_L|$ are: (a) $n_{\max} = 8, \varepsilon_1 = 13.58$ m, (b) $n_{\max} = 10, \varepsilon_1 = 2.58$ m, (c) $n_{\max} = 12, \varepsilon_1 = 7.58$ m, (d) $n_{\max} = 14, \varepsilon_1 = 6.58$ m, (e) $n_{\max} = 16, \varepsilon_1 = 2.58$ m, (f) $n_{\max} = 18, \varepsilon_1 = 3.58$ m, (g) $n_{\max} = 20, \varepsilon_1 = 6.58$ m, (h) $n_{\max} = 22, \varepsilon_1 = 9.58$ m. As concluded from the previous experiment, the influence of noise on the identification results is remarkable. This brings about a trade-off between the use of more harmonics and localization accuracy. Higher harmonics are prone to higher noise levels as can be observed in Figs. 12 and 15. As a consequence, the use of high frequency information –which are extremely noisy– cannot add new information and would even cause to corrupt the results by imposing noise-induced oscillations on the identification procedure.

In order to give an overview of the localization performance, the simulated pressure-head spectrum corresponding to the estimated leak properties (plotted in continuous red) and those corresponding to the actual leak location and size (displayed in dashed blue) are compared in Fig. 17a for $n_{\max} = 12$ and Fig. 17b for $n_{\max} = 22$. Similar to what was shown for the previous experiment, a good agreement between these two curves is observed which implies that the method performs well. However, a more advanced methodology to tackle the unsteady friction (e.g. [60]), viscoelasticity (e.g. [41]), pump action, linearization errors [53] and perhaps other transient phenomena (e.g. [54] or Fluid-Structure Interaction as argued in [55, 56]) is sought so as to arrive

at an improved agreement with the measurements and hence enhance the localization. Besides, as pointed out in [9, 33, 50, 57], the calibrated creep coefficients can significantly affect the leak identification, therefore a particular attention should be dedicated to their precise estimation.

Table 2. Pipe and flow specifications of the HKUST experiment [33, 35].

$D = 79.2$ mm	$J_0 = 1.5 \times 10^{-9}\text{Pa}^{-1}$	$\tau_1 = 0.0377$ s	$J_1 = 0.076 \times 10^{-9}\text{Pa}^{-1}$
$\tau_2 = 0.7304$ s	$J_2 = 0.085 \times 10^{-9}\text{Pa}^{-1}$	$\tau_3 = 1.4968$ s	$J_3 = 1.105 \times 10^{-9}\text{Pa}^{-1}$
$\tau_4 = 5.3073$ s	$J_4 = 0.053 \times 10^{-10}\text{Pa}^{-1}$	$\tau_5 = 10.582$ s	$J_5 = 0.905 \times 10^{-10}\text{Pa}^{-1}$
$H_U = 45.4$ m	$Q_0 = 0.5$ L/s	$\rho = 1000$ kg/m^3	$\kappa = 2.1$ GPA

It is worth to emphasize here that the proposed method is also able to perform localization using multiple spatial measurements if several (N_s) sensors as defined in Eq. (23) are deployed to collect transient data. However, in real practice, it is more convenient to repeat a test and compute the mean signal so as to reduce the noise variance and raise the accuracy. More specifically, let the vector $\overline{\mathbf{h}^M}$ (with each entries being shown by $\overline{h_k^M}$) denote the mean of S measurements (i.e. statistically independent random vectors $\mathbf{h}^{Mi}, i = 1,2, \dots, S$) all with the same variance σ^2, then

$$\text{Var}\left(\overline{h_k^M}\right) = \text{Var}\left(\frac{1}{S}\sum_{i=1}^{S} h_k^{Mi}\right) = \frac{1}{S^2}\sum_{i=1}^{S} \text{Var}(h_k^{Mi}) = \frac{\sigma^2}{S} \tag{31}$$

which means that by repeating an experiment for S times, the variance of the mean signal reduces by $1/S$. As a consequence, the proposed methodology facilitates a localization exercise by making possible to identify leaks without the need for collecting measurements at three different spatial stations; when more accuracy matters, repeating the transient test is the best advice.

The Cramer Rao Lower Bound (CRLB) of a leak location estimator which yields the minimum variance of identified leak locations provides marginal gain obtained by repeating a transient test, deploying further sensors or variation of other physical parameters [30, 46]. For the old method in a frictionless system it reads [30]

$$\mathrm{CRLB}(z_L) = \mathrm{Var}(\hat{z}_L) = \frac{H_L^0 \sigma^2}{S A_e^2 g \vartheta^4 \sum_{j=1}^{J} \left((q_{Uj}^M)^2 \sin^2 \left(\frac{\omega_j}{a} (z_m - 2z_L) \right) \right)}, \qquad \vartheta = \frac{a}{gA} \tag{32}$$

in which S = sample size (number of times the experiment is repeated); z_m = measurement location; A_e = effective leak area; σ^2 = noise; A = cross-sectional area of flow; H_L^0 = steady-state pressure head at the leak; ω_j = jth selected angular frequency for leakage detection ($j = 1,2, \dots, J$); and q_{Uj}^M = jth amplitude of transient flow rate at upstream. This relation explicitly reveals that repeating an experiment can reduce the variance of localization by a $1/S$ or cut down the root mean square error by a factor of $\sqrt{S}$ as already discussed. Besides, it implies that one can hardly claim that collecting data at two distinct locations is beneficial in general because to maximize the denominator (to minimize the CRLB), the sine term should be maximized which itself depends on the leak location being a priori unknown. This supports the argument that collecting transient data at various spatial stations rather than repeating transients at identical locations, cannot be significantly advantageous. Accordingly, the proposed formulation not only has all credits of the previous method, but also is capable of identification using a single measurement with great accuracy (if the measured signal is enhanced by repeating tests).

6. Conclusions

This research reformulates the recently established spectral-based leak identification method called MFP or MLE in order to enable them find leaks with much less information. In contrast to the conventional leak-identification approach which requires at least measured spectra of three stations, the developed formulation allows to pinpoint leaks using a single transient spectrum. This is accomplished by efficient application of the transfer matrices exploited in the objective function. The rationale behind this achievement is clear for example in a reservoir-pipe-valve system: in the forward problem, the transient pressure and flow rate at either boundaries are determined if all system properties (specifically leaks) are known; as a consequence, in the identification (inverse) problem, when leak properties are unknown, the measured data only at a single station must be enough to compensate for the unavailable leak data and hence the analysis of the system. Furthermore, the time domain methods identify leaks with a single measurement.

The concluding remarks consisting of comparison between the proposed (new) and the conventional (old) method, the experimental verifications and future perspectives can be outlined as follows.

- Theoretical expressions giving rise to the merit function of each method are of similar form, however, their definitions differ; the old one is based on discharge and pressure measurements and the new method only incorporates single pressure spectrum or more (optional).
- A comparison of the two methods reveal that both are robust to pinpoint one leak. However, the new method outweighs the first one as it suppresses the side lobes to a greater extent. This is highly desirable especially in cases of high noise level or multiple leaks which are widespread in real practice.

- Numerical investigations demonstrated that the new method is more stable subject to extreme noise levels. This is also supported by theoretical evidence showing that the merit function of the proposed method has smaller variance.
- An assessment of the performance of the two methods in localizing two leaks revealed that the new method outweighs the old one on average when several leak positions are tested.
- When it comes to localization with high level of accuracy, deploying several sensors to collect transient data at different locations is an option. With such data, both methods can provide satisfactory results. However, another more convenient option – that only the proposed method can apply – is to collect data of a transient test at a single station, then repeat the test and compute the mean signal to decline the variance of measurement thus escalating the accuracy.
- The suggested formulation sheds new lights on improved identification of multiple leaks based on multi-leak models using a single spatial measurement.

ACKNOWLEDGEMENTS

This work has been supported by the Hong Kong Research Grants Council (RGC) under the General Research Fund (GRF) Projects (no. 15200719 and no. 15201017) and the Theme-based Research Scheme (TRS) project (no. T21-602/15R). The University of Perugia and The Hong Kong University of Science and Technology are acknowledged for generating the experimental data for the collaborative TRS project.

7. Appendix A. Derivation of Eq. (8)

The matrix-product operations making up to the transfer matrix can be simplified in view of Eq. (5) as follows

$$\mathbf{T} = \mathbf{M}^{NL}_{z_m - z_L} \begin{bmatrix} 1 & \alpha_L \\ 0 & 1 \end{bmatrix} \mathbf{M}^{NL}_{z_L - z_U} = \mathbf{M}^{NL}_{z_m - z_L} (\mathbf{I} + \mathbf{L}) \mathbf{M}^{NL}_{z_L - z_U}$$

$$= \mathbf{M}^{NL}_{z_m - z_L} \mathbf{M}^{NL}_{z_L - z_U} + \alpha_L \, \mathbf{M}^{SL}_{z_L} \tag{A1}$$

$$= \mathbf{S}\mathbf{E}_{z=z_m - z_L} \mathbf{S}^{-1} \mathbf{S}\mathbf{E}_{z=z_L - z_U} \mathbf{S}^{-1} + \alpha_L \, \mathbf{M}^{SL}_{z_L} = \mathbf{M}^{NL}_{z_m - z_U} + \alpha_L \mathbf{M}^{SL}_{z_L},$$

$$\mathbf{M}^{SL}_{z_L} = \mathbf{M}^{NL}_{z_m - z_L} \, \mathbf{L} \, \mathbf{M}^{NL}_{z_L - z_U}, \quad \mathbf{L} = \begin{bmatrix} 0 & 1 \\ 0 & 0 \end{bmatrix},$$

8. Appendix B. Measured signals used for leak detection

In any leak detection exercise, the collected transient data are key for a successful result. In the spectral based methods, the collected transient data which are usually available in the time domain need to be transformed to the frequency domain. For the numerical test presented in Section 4.1, the required time domain measurements (noise-free) are shown in Fig. 18. The new method identifies leaks only based on this signal but the old method requires two additional measurement vectors.

The time series data presented in Fig. 18 transform to complex spectra whose real and imaginary parts are shown in Fig. 19a, b, and their absolute values are depicted in Fig. 20. A comparison between the pressure response of the intact and the leaky pipe system indicate that leak location

and size can be identified by the travel time and the magnitude of the reflected wave in the time-domain methods (Fig. 18), and the pattern (leak location) and the variations magnitude (leak size) of resonant peaks in the spectral-based methods. The proposed method efficiently applies the latter characteristics to pinpoint the leak.

9. Nomenclature

The following symbols are used in this paper:

$\mathbf{n}$ noise vector

$\mathbf{h}^M$ measured pressure head

$\mathbf{q}_U^M$ measured flow rate at the upstream

$\mathbf{Y}$ unknown vector

$\mathbf{T}$ transfer function

$\mathbf{A}, \mathbf{B}$ coefficient matrices of the system equation

a pressure wave speed

h pressure head amplitude

J creep function

ρ density

s Laplace variable

z axial coordinate of pipe

q cross-sectional flow rate

g gravitational acceleration

D inner diameter of the pipe

e pipe wall thickness

t time

τ retardation time

f friction factor

α_L characteristic leak size

z_L leak location coordinate

$\mathbf{a}_i$ eigenvalues of the matrix $\mathbf{A^{-1}B}$

E elastic modulus of the pipe wall

Subscripts

j frequency index

m measurement-station node

k data index

Superscripts

D downstream node

NL no leak

SL single leak

H conjugate transpose

U upstream node

Acronyms

MFP = Matched Field Processing

MLE = Maximum Likelihood Estimation

RMSE = Root Mean Square Error

SNR = Signal to Noise Ratio

TMM = Transfer Matrix Method

VE = Viscoelasticity

10. REFERENCES

[1] Colombo, A.F., Lee, P., and Karney, B.W. (2009). A selective literature review of transient-based leak detection methods. Journal of Hydro-environment Research, Vol.2(4), 212-227.

[2] Keramat, A., Payesteh, M., Brunone, B., Meniconi, S., (2020). Interdependence of Flow and System Characteristics in Transient Induced Contamination Intrusion in Pipes: Numerical Analysis. Journal of Hydroinformatics, IWA publishing https://doi.org/10.2166/hydro.2020.069

[3] Ghorbanian, V., Karney, B., Guo, Y. (2017) Intrinsic relationship between energy consumption, pressure, and leakage in water distribution systems, Urban Water Journal, 14:5, 515-521, DOI: 10.1080/1573062X.2016.1223325

[4] Xu, X., and Karney, B. (2017). An overview of transient fault detection techniques. In Modeling and Monitoring of Pipelines and Networks, C. Verde and L. Torres (eds.), Springer Int. Publishing, 13-37.

[5] Liggett, J. A., and Chen, L.C. (1994). Inverse transient analysis in pipe networks. Journal of Hydraulic Engineering. 1208, 934–955.

[6] Brunone, B. (1999). Transient test-based technique for leak detection in outfall pipes. Journal of Water Resources Planning and Management, 125(5), 302-306.

[7] Meniconi, S., Brunone, B., Ferrante, M., and Massari, C. (2011). Transient tests for locating and sizing illegal branches in pipe systems. Journal of Hydroinformatics, IWA, 13(3), 334-345.

[8] Misiunas, D., Vítkovský, J., Olsson, G., Simpson, A., and Lambert, M. (2005). Pipeline break detection using transient monitoring. Journal of Water Resources Planning and Management, 131(4), 316-325.

[9] Keramat, A., Louati, M., Wang, X., Meniconi, S., Brunone, B., Ghidaoui, M.S., Objective Functions for Transient-Based Pipeline Leakage Detection in a Noisy Environment: Least Square and Matched-Filter. Journal of Water Resources Planning and Management, ASCE (2019). DOI: 10.1061/(ASCE)WR.1943-5452.0001108

[10] Vítkovský, J. P., Simpson, A. R., and Lambert, M. F. (2000). Leak detection and calibration using transients and genetic algorithms. J. Water Resour. Plann. Manage., 126(4), 262–265.

[11] Vítkovský, J.P., Lambert, M., Simpson, A., and Liggett, J. (2007). Experimental Observation and Analysis of Inverse Transients for Pipeline Leak Detection. Journal of Water Resources Planning and Management, 133(6), 519-530.

[12] Covas, D., and Ramos, H. (2010). Case Studies of Leak Detection and Location in Water Pipe Systems by Inverse Transient Analysis. Journal of Water Resources Planning and Management, 136(2), 248–257.

[13] Brunone, B., and Ferrante, M. (2001). Detecting leaks in pressurized pipes by means of transients. Journal of Hydraulic Research 39(5), 539–547.

[14] Mpesha, W., Gassman, S.L., and Chaudhry, M.H. (2011). Leak detection in pipes by frequency response method. Journal of Hydraulic Engineering, 127(2), 134-147.

[15] Kim, S.H. (2005). Extensive development of leak detection algorithm by impulse response method. Journal of Hydraulic Engineering, 131(3), 201-208.

[16] Lee P, Vitkovsky J, Lambert M, Simpson A, and Liggett J. (2005). Frequency domain analysis for detecting pipeline leaks. J Hydraul Eng ASCE 131(7):596–604.

[17] Lee, P.J, Vítkovský, J.P., Lambert, M.F., Simpson, A.R., and Liggett, J. (2005). Leak location using the pattern of the frequency response diagram in pipelines: a numerical study. Journal of Sound and Vibration, 284(3), 1051-1073.

[18] Duan, H.-F, Lee, P.J., Ghidaoui, M.S., and Tung, Y.K. (2011). Leak detection in complex series pipelines by using the frequency response method. Journal of Hydraulic Research, 49(2), 213-221.

[19] Lee, P.J., Duan, H.-F, Ghidaoui, M., and Karney, B. (2013). Frequency Domain Analysis of Pipe Fluid Transient Behaviour. Journal of Hydraulic Research, 51(6), 609-622.

[20] Lee P, Vitkovsky J, Lambert M, Simpson A, and Liggett J. (2007). Leak location in pipelines using the impulse response function. Journal of Hydraulic Research, IAHR 45(5):643–652.

[21] Covas, D., Ramos, H., Almeida, A.B., 2005. Standing wave difference method for leak detection in pipeline systems. Journal of Hydraulic Engineering, ASCE 131 (12), 1106-1116.

[22] Wang X.J., Lambert M.F., Simpson A.R., Liggett J.A. and Vítkovský J.P. (2002). Leak detection in pipelines using the damping of fluid transients. Journal of Hydraulic Engineering, 128:697-711. DOI: 10.1061/(ASCE)0733-9429(2002)128:7(697)

[23] Gong, J., Lambert, M.F., Zecchin A.C., Simpson A.R., 2016. Experimental verification of pipeline frequency response extraction and leak detection using the inverse repeat signal, Journal of Hydraulic Research, 54, 210-219.

[24] Duan, H.-F. 2015. Uncertainty analysis of transient flow modeling and transient-based leak detection in elastic water pipeline systems, Water Resour. Manage. 29, 5413–5427.

[25] Kim S. H. 2020. Multiple leak detection algorithm for pipe network. Mechanical Systems and Signal Processing, 139, 106645. DOI: 10.1016/j.ymssp.2020.106645.

[26] Pan, B., Duan, H.-F, Meniconi, S., and Brunone, B. 2021. FRF-based transient wave analysis for the viscoelastic parameters identification and leak detection in water-filled plastic pipes. Mechanical Systems and Signal Processing, 146, 107056. DOI: 10.1016/j.ymssp.2020.107056)

[27] Duan, H.-F, 2018. Accuracy and sensitivity evaluation of TFR method for leak detection in multiple pipeline water supply systems, Water Resour. Manage. 32, 2147–2164.

[28] Duan, H.-F., (2017). Transient frequency response based leak detection in water supply pipeline systems with branched and looped junctions, J. Hydroinf. 19, 17–30.

[29] Wang, X., and Ghidaoui, M.S., (2018a). Pipeline leak detection using the matched-field processing method. Journal of Hydraulic Engineering, ASCE, 144(6), 04018030.

[30] Wang, X., and Ghidaoui, M.S., (2018b). Identification of multiple leaks in pipeline: linearized model, maximum likelihood, and super-resolution localization. Mechanical Systems and Signal Processing, 107, 529-548.

[31] Wang, X., Palomar, D. P., Zhao, L., Ghidaoui, M. S., and Murch, R. D. (2019) Spectral-based methods for pipeline leak detection, Journal of Hydraulic Engineering, ASCE, In press. DOI: 10.1061/(ASCE)HY.1943-7900.0001572

[32] Wang, X., and Ghidaoui, M.S., (2019). Identification of multiple leaks in pipeline II: Iterative beamforming and leak number estimation. Mechanical Systems and Signal Processing, 119, 346-362.

[33] Wang, X., Lin, J., Keramat, A., Ghidaoui, M.S., Meniconi, S., and Brunone, B. (2019) Matched-field processing for leak localization in a viscoelasticity pipe: An experimental study, Mechanical Systems and Signal Processing, vol. 124, pp. 459-478.

[34] Wang, X., Waqar, M., Yan, H.C., Louati, M., Ghidaoui, M.S., Lee, P.J., Meniconi, S., Brunone, B., Karney, B. (2020). Pipeline leak localization using matched-field processing incorporating prior information of modeling error, Mechanical Systems and Signal Processing, Vol. 143. https://doi.org/10.1016/j.ymssp.2020.106849.

[35] Wang, X., Ghidaoui, M.S., and Lin, J., Identification of multiple leaks in pipeline III: Experimental results, Mechanical Systems and Signal Processing, vol. 130, pp. 395-408, 2019

[36] Prek, M., 2007. Analysis of wave propagation in fluid-filled viscoelastic pipes. Mech. Syst. Signal Process. 21, 1907–1916. https://doi.org/10.1016/j.ymssp.2006.07.013

[37] Chaudhry, M.H., 2014. Applied Hydraulic Transients, Third. ed. Springer. https://doi.org/10.1007/978-1-4614-8538-4

[38] Covas, D., Stoianov, I., Mano, J., Ramos, H., Graham, N., and Maksimovic, C. (2005). The dynamic effect of pipe-wall viscoelasticity in hydraulic transients. Part II–model development, calibration and verification. Journal of Hydraulic Research 43, 56–70.

[39] Covas, D., Stoianov, I., Mano, J.F., 2004. The dynamic effect of pipe-wall viscoelasticity in hydraulic transients. Part I - Experimental analysis and creep characterization. Hydraul. Res. 42, 517–531.

[40] Keramat, A., Tijsseling, A.S., Waterhammer with column separation, fluid-structure interaction and unsteady friction in a viscoelastic pipe, 11th International Conference on, Pressure Surges Lisbon, October 24- 26, 2012.

[41] Keramat, A., Gaffarian Kolahi, A., Ahmadi, A., Waterhammer modelling of viscoelastic pipes with a time-dependent Poisson's ratio, Journal of Fluids and Structures, 43 (2014) 164-178.

[42] Keramat, A., Haghighi A., Straightforward Transient-Based Approach for the Creep Function Determination in Viscoelastic Pipes, Journal of Hydraulic Engineering, ASCE, (2014), 140(12) 04014058.1-04014058.9.

[43] Karimian Aliabadi H, Ahmadi A, Keramat A. Frequency response of water hammer with fluid-structure interaction in a viscoelastic pipe. Mechanical Systems and Signal Processing, 144(2020), 106848.

[44] Keramat, A., Tijsseling, A.S., Hou, Q., Ahmadi, A. (2012). Fluid-structure interaction with pipe-wall viscoelasticity during water hammer. Journal of. Fluids and Structures 28, 434–455.

[45] Casella, G., and R. L. Berger. 2002. Statistical inference. 2nd ed. Pacific Grove, CA: Duxbury/Thomson Learning.

[46] Keramat, A., Ghidaoui, M., Wang, X., and Louati, M. (2018). Cramer-Rao lower bound for performance analysis of leak detection. Journal of Hydraulic Engineering, ASCE. DOI: 10.1061/(ASCE)HY.1943-7900.0001603

[47] Keramat, A., Zanganeh, R., Statistical performance analysis of transient-based extended blockage detection in a water supply pipeline. Journal of Water Supply: Research and Technology-Aqua jws2019014. (2019). https://doi.org/10.2166/aqua.2019.014.

[48] Louati, M., Ghidaoui, M.S., Tekitek, M.M., Lee, P.J., (2020). Wave-Leak Interaction in a Simple Pipe System. Journal of Hydraulic Engineering, ASCE. 146(4) DOI: 10.1061/(ASCE)HY.1943-7900.0001714

[49] Lee, P.J., Duan, H.-F, Tuck, J., and Ghidaoui., M. (2015). Numerical and Experimental Study on the Effect of Signal Bandwidth on Pipe Assessment using Fluid Transients. Journal of Hydraulic Engineering, ASCE 141 (2): 04014074. DOI: 10.1061/(ASCE)HY.1943-7900.0000961

[50] Wang, X., Lin, J., Ghidaoui, M.S., Meniconi, S., Brunone, B. (2020). Estimating viscoelasticity of pipes with unknown leaks, Mech. Syst. Signal Process. 143, 106821.

[51] Gong, J., Zecchin, A.C., Lambert, M.F., Simpson, A.R. (2016). Determination of the creep function of viscoelastic pipelines using system resonant frequencies with hydraulic transient analysis, J. Hydraul. Eng. 142 (2016) 04016023

[52] Pan, B., Duan, H.-F, Meniconi, S., Urbanowicz, K., Che, T., Brunone, B. 2020. Multistage frequency-domain transient-based method for the analysis of viscoelastic parameters of plastic pipes, J. Hydraul. Eng. 146, 04019068.

[53] Ranginkaman, M.H., Haghighi, A., Lee, P.J. 2019. Frequency domain modelling of pipe transient flow with the virtual valves method to reduce linearization errors, Mech. Syst. Sig. Process. 131, 486–504.

[54] Keramat, A., Heidari Shirazi, K., 2014. Finite element based dynamic analysis of viscoelastic solids using the approximation of Volterra integrals, Finite Elements in Analysis and Design, 86, 89-100. DOI: 10.1016/j.finel.2014.03.010.

[55] Zanganeh, R., Jabbari, E., Tijsseling, A., Keramat, A., 2020. Fluid-Structure Interaction in Transient-Based Extended-Defect Detection of Pipe Walls. Journal of Hydraulic Engineering, ASCE, 146(4).

[56] Keramat, A., Fathi-Moghadam, M., Zanganeh, R., Rahmanshahi, M., Tijsseling, A.S., Jabbari, E., (2020). Experimental investigation of transients-induced fluid–structure interaction in a pipeline with multiple-axial supports, Journal of Fluids and Structures, 93. 102848. https://doi.org/10.1016/j.jfluidstructs.2019.102848.

[57] Brunone, B., Meniconi, S., and Capponi, C. (2018). Numerical analysis of the transient pressure damping in a single polymeric pipe with a leak. Urban Water Journal. DOI: 10.1080/1573062X.2018.1547772.

[58] Zhang, C., Lambert, M.F., Gong, J., Zecchin, A.C., Simpson A.R., Stephens, M.L., (2020) Bayesian Inverse Transient Analysis for Pipeline Condition Assessment: Parameter Estimation and Uncertainty Quantification. Water Resour Manage. https://doi.org/10.1007/s11269-020-02582-9

[59] Zhang C., Gong J., Lambert M.F., Simpson A.R., Zecchin, A.C. (2019) Sensor placement strategy for pipeline condition assessment using inverse transient analysis. Water Resour Manag 33(8):2761–2774

[60] Kim, S. H. (2011). Holistic Unsteady Friction Model for the Laminar Transient Flow in Pipeline Systems. Journal of Hydraulic Engineering, 127(120), 1649-1658.

11. Figures

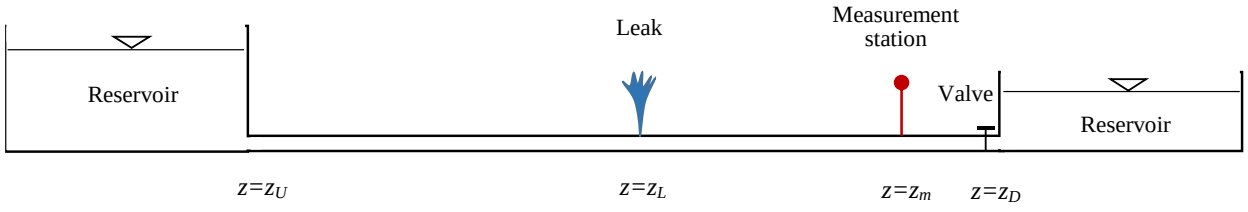

Fig 1 The schematic of the pipeline in a typical reservoir-leaky pipeline-valve system considered for leak identification.

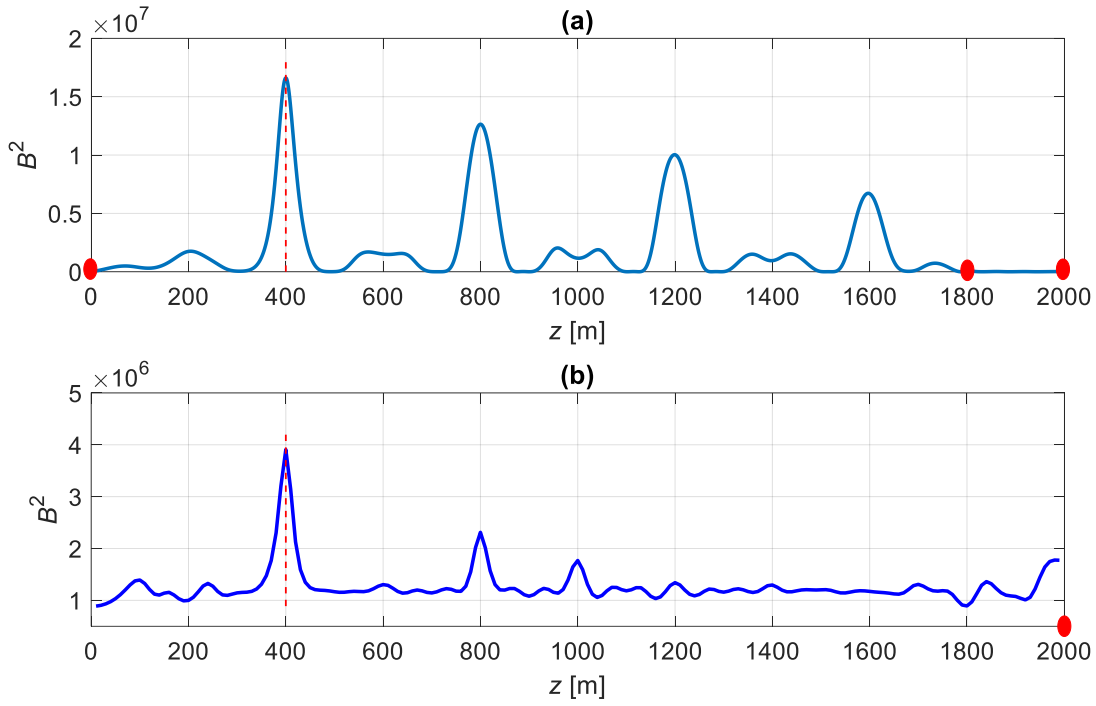

Fig 2 Localization of a single leak by plotting the objective function using the two methods (a) old method requiring measurements at least at three locations and (b) new method which is capable of localization using a single spectrum (single spatial sensor); the dashed line and the ellipses on the horizontal axes indicate the location of the leak and measurement stations, respectively.

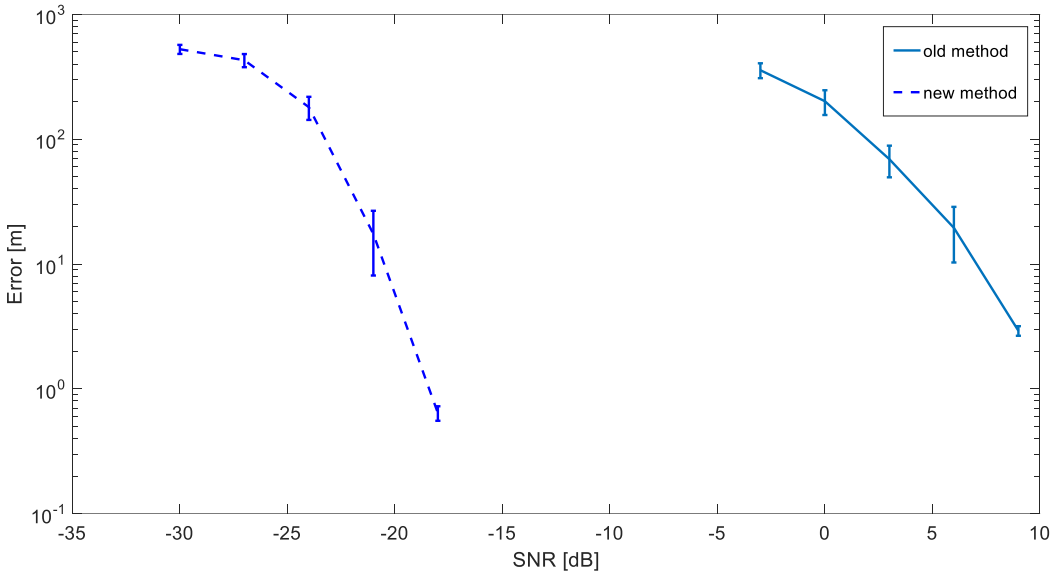

Fig 3 Mean and 95% confidence interval of localization error for the old method (continuous line) and new method (dashed line).

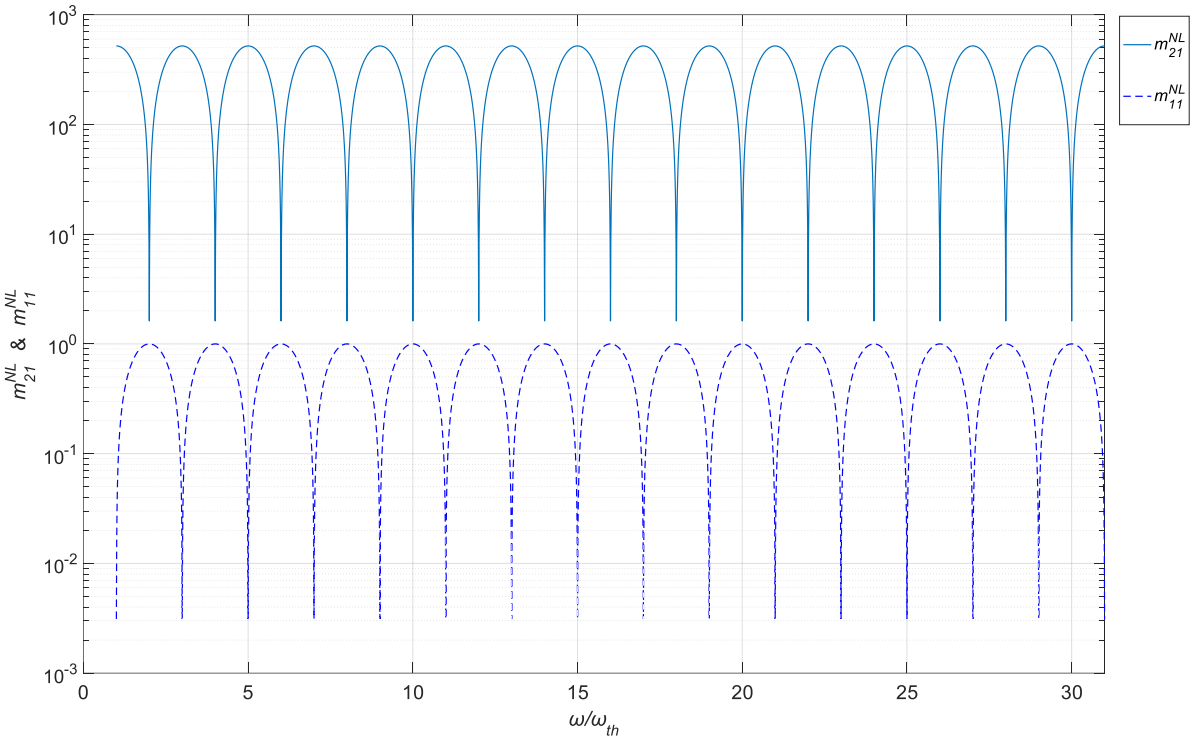

Fig 4 Representation of the values of m_{21}^{NL} and m_{11}^{NL} used to estimate Δh_k in the old and new method, respectively.

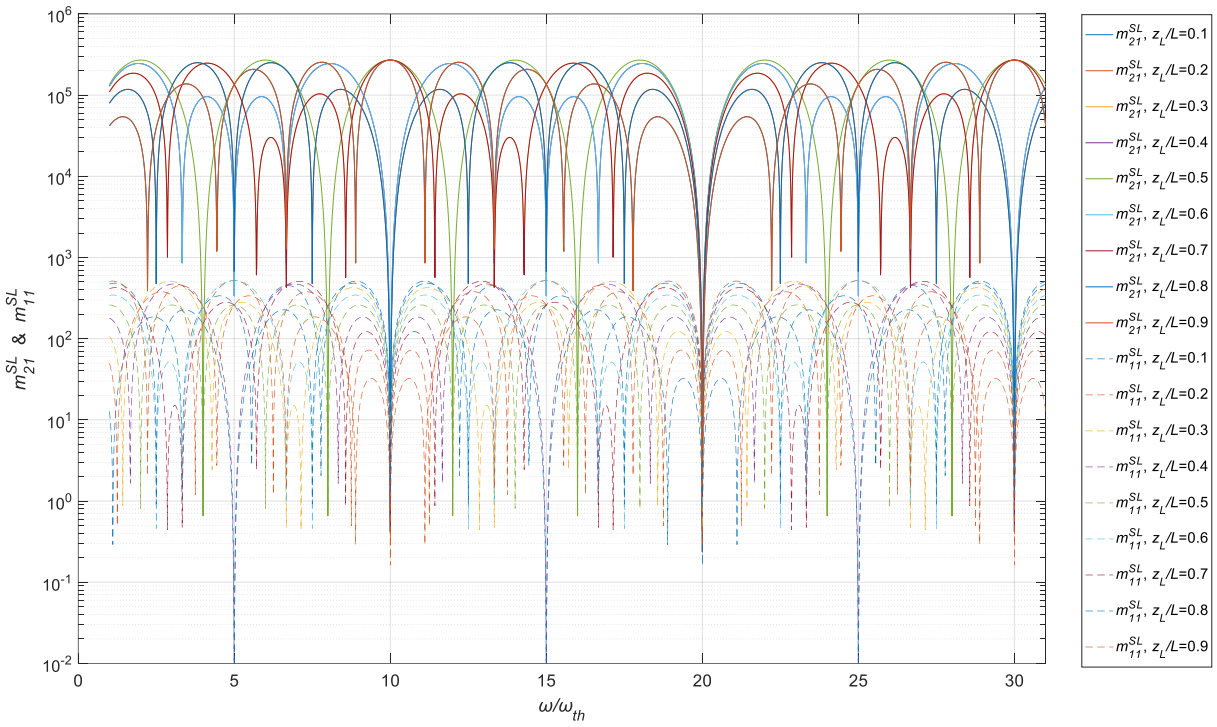

Fig 5 Representation of the values of m_{21}^{SL} and m_{11}^{SL} used to estimate G_k in the old and new method, respectively.

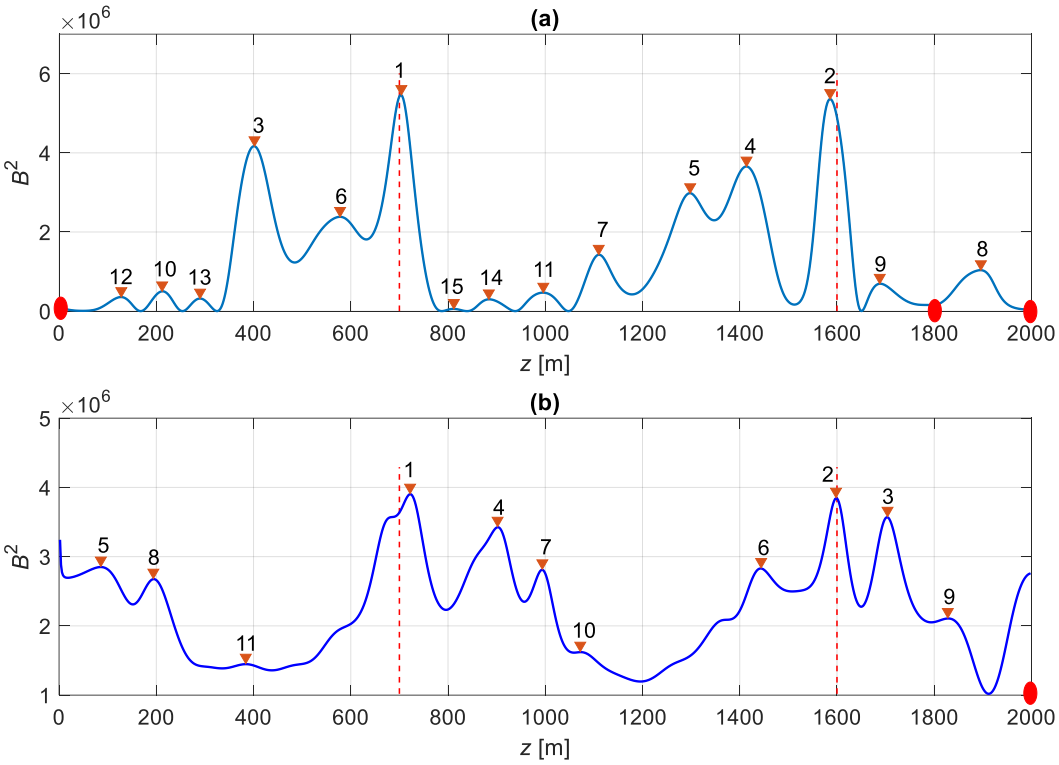

Fig 6 Localization of two leaks by plotting the objective function for frequencies $\omega = \{n\omega_{th} : n = 1,2, \dots ,31\}$ using the two methods (a) old and (b) new method; the dashed line, the ellipses and the triangles indicate the location of the leak, measurement stations and local maxima, respectively.

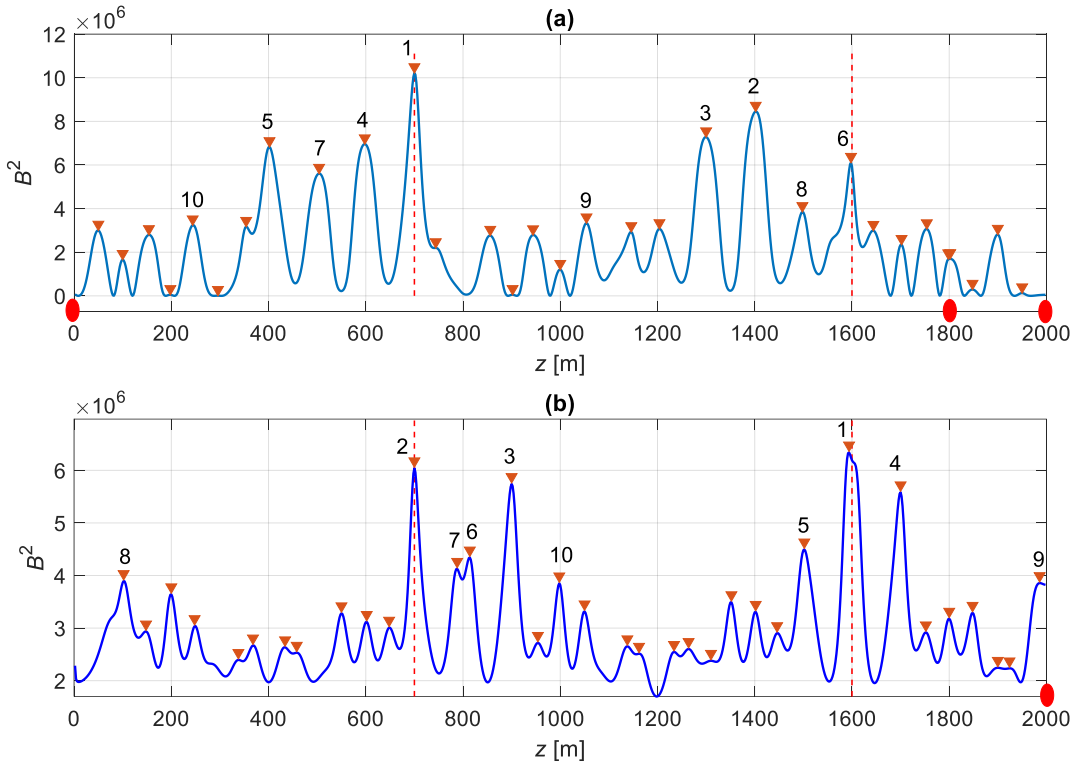

Fig 7 Localization of two leaks by plotting the objective function for frequencies $\omega = \{n\omega_{th} : n = 1,2,\dots,51\}$ using the two methods (a) old method, (b) new method; the dashed line, the ellipses and the triangles indicate the location of the leak, measurement stations and local maxima, respectively

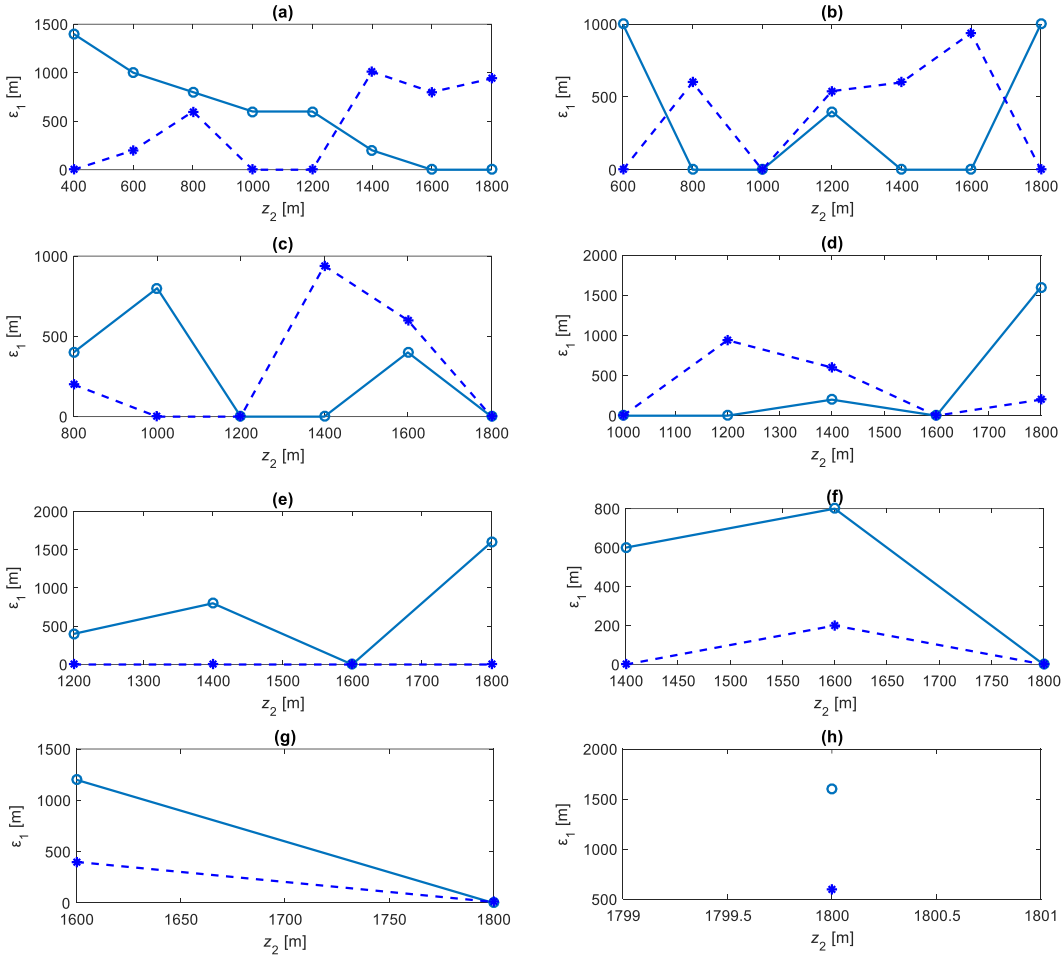

Fig 8 Estimated error of localization (ε_1) against various positions of the second leak (z_2) using the old method (continuous line) and the new method (dashed line) for various locations of the first leak: (a) $z_1 = 200$ m, (b) $z_1 = 400$ m, (c) $z_1 = 600$ m, (d) $z_1 = 800$ m, (e) $z_1 = 1000$ m, (f) $z_1 = 1200$ m, (g) $z_1 = 1400$ m, (h) $z_1 = 1600$ m. SNR = 100 dB.

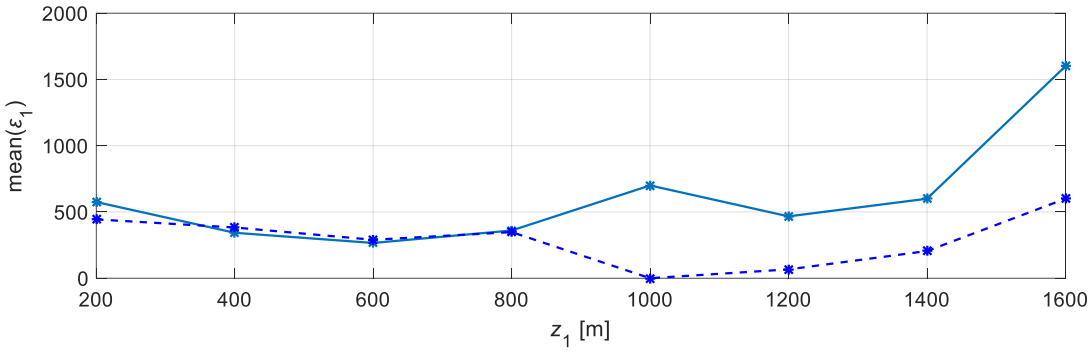

Fig 9 The estimated mean of ε_1 (plotted in Fig. 8) when it is averaged over all estimations of the second leak (z_2) for a fixed z_1 indicated in the horizontal axis, for the old method (continuous line) and new method (dashed line).

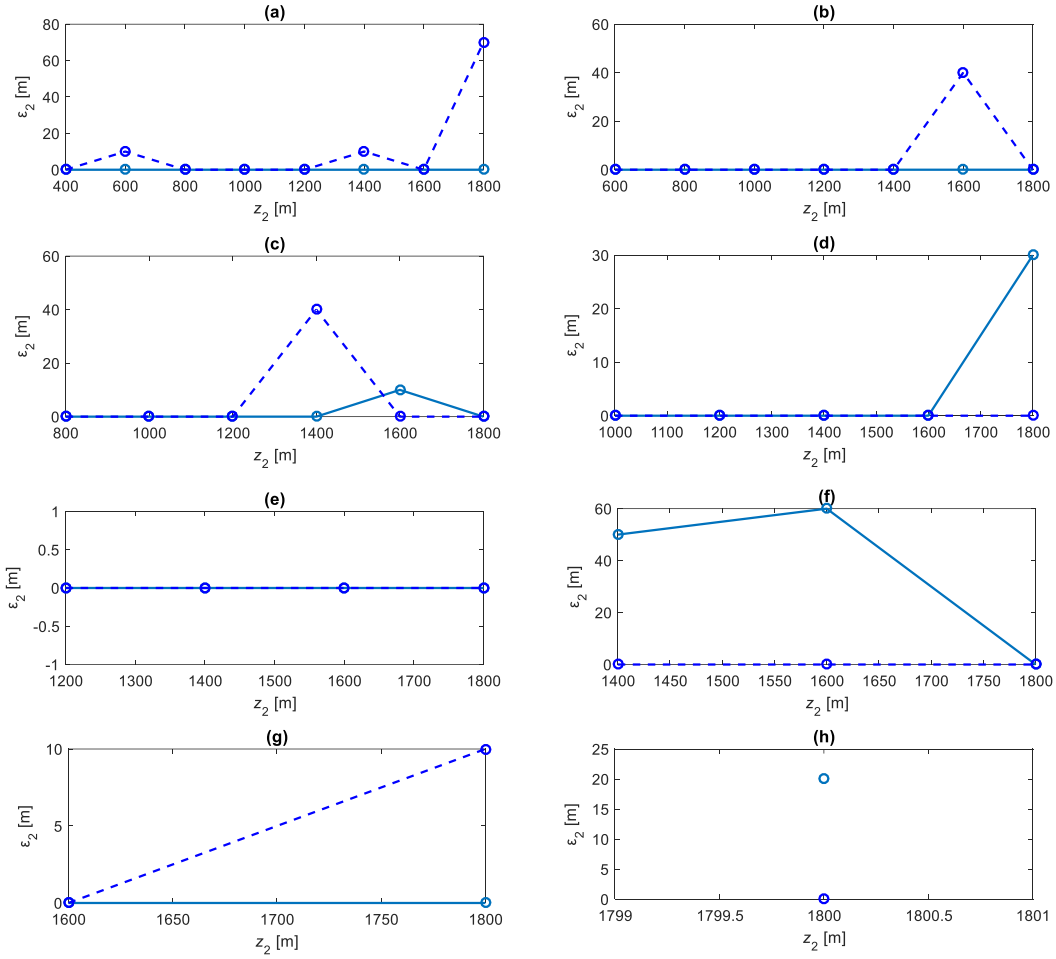

Fig 10 Estimated error of localization (ε_2) against the positions of the second leak (z_2) using the old method (continuous line) and the new method (dashed line) for various locations of the first leak: (a) $z_1 = 200$ m, (b) $z_1 = 400$ m, (c) $z_1 = 600$ m, (d) $z_1 = 800$ m, (e) $z_1 = 1000$ m, (f) $z_1 = 1200$ m, (g) $z_1 = 1400$ m, (h) $z_1 = 1600$ m.

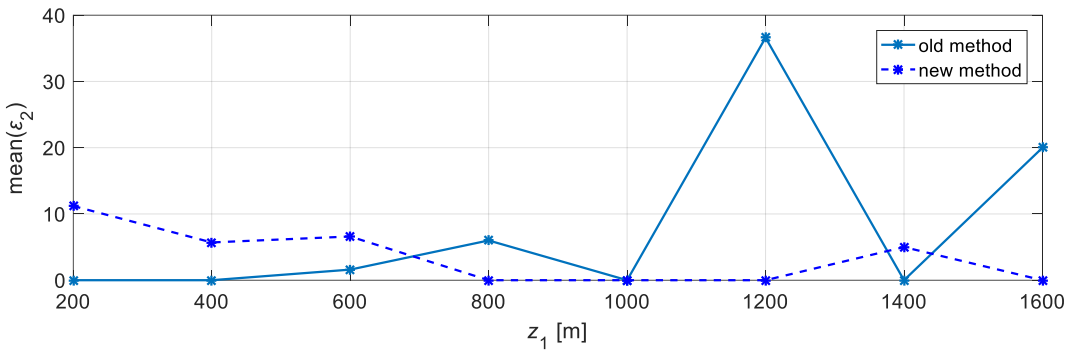

Fig 11 The estimated mean of ε_2 (plotted in Fig. 10) when it is averaged over all estimations of the second leak (z_2) for a fixed z_1 indicated in the horizontal axis, for the old method (continuous line) and new method (dashed line).

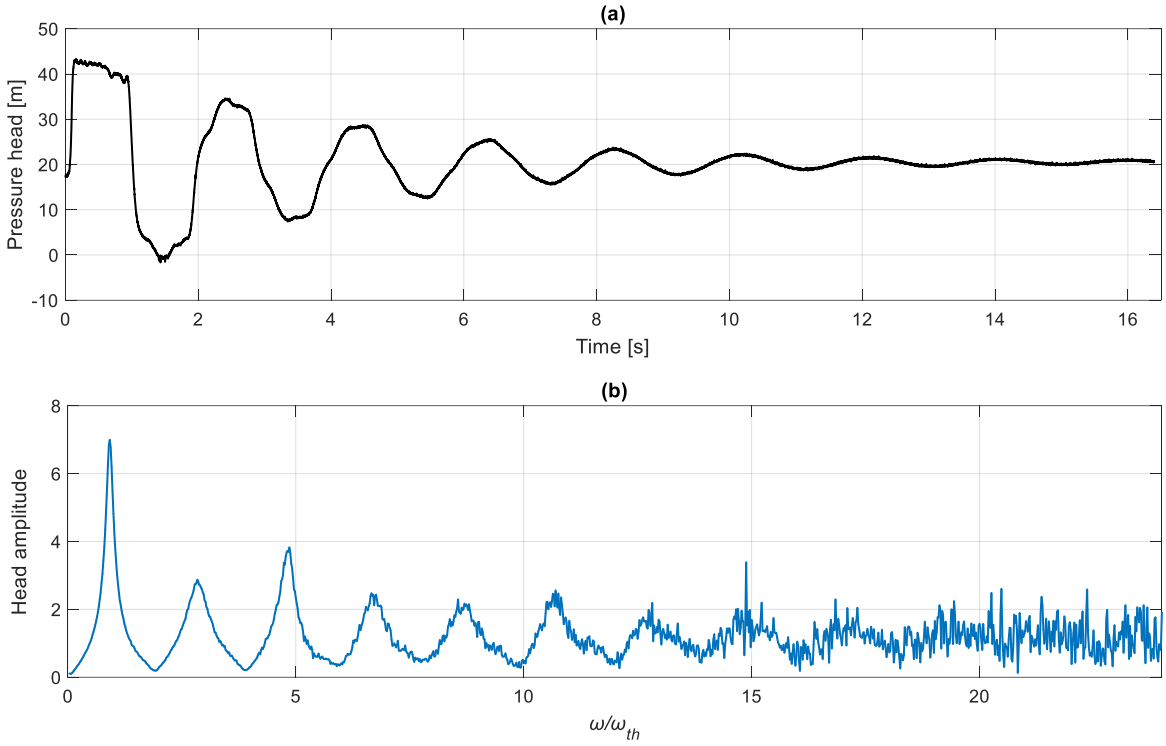

Fig 12 Measurements of pressure head at the downstream valve in the Perugia experiment; (a) time domain, and (b) frequency domain data.

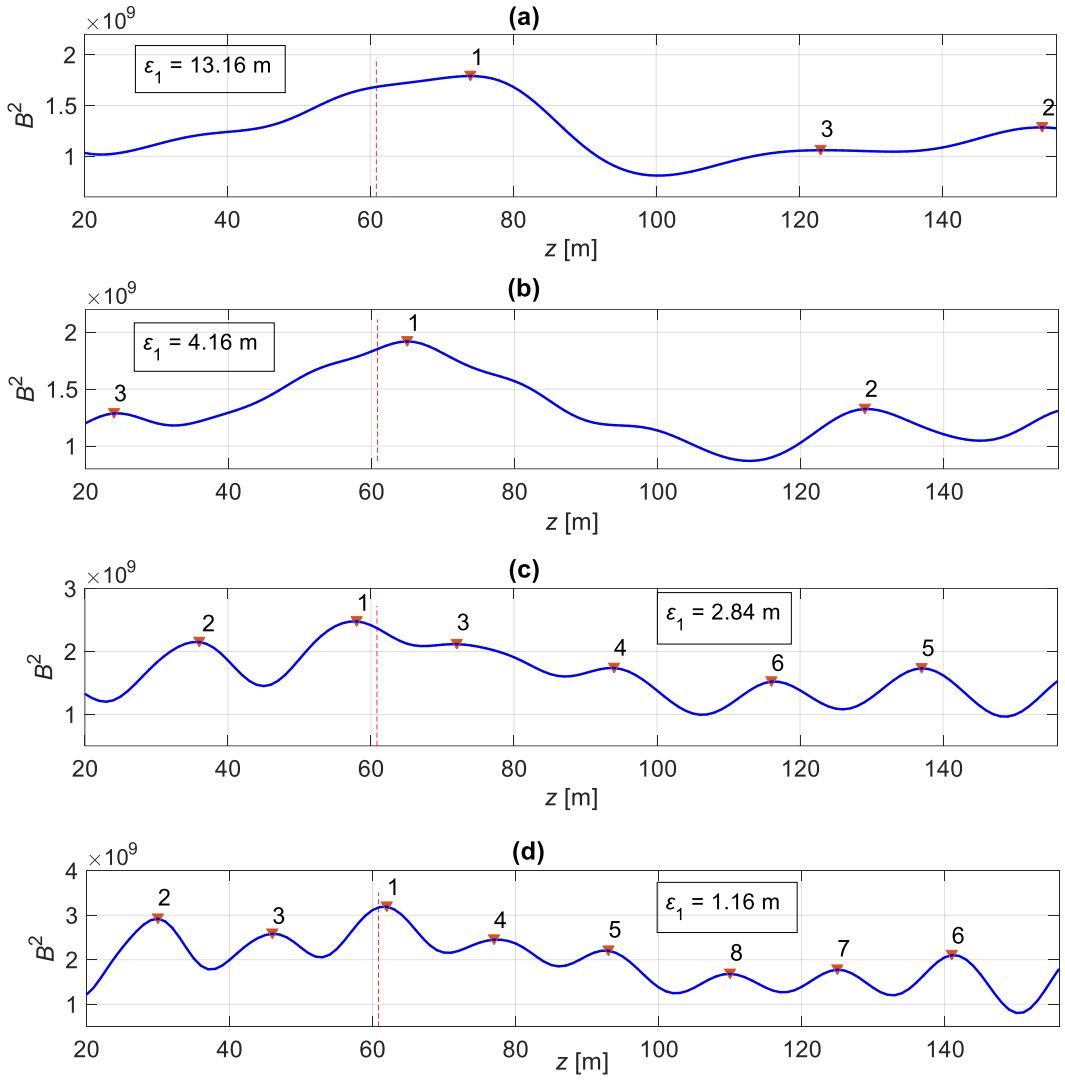

Fig 13 Localization results of the proposed method for the Perugia experiment when different signal bandwidth $\omega = \omega_{th} \times (1{:}\,0.01{:}\,n_{\max})$ is incorporated: (a) $n_{\max} = 8$, (b) $n_{\max} = 12$, (c) $n_{\max} = 16$, (d) $n_{\max} = 20$.

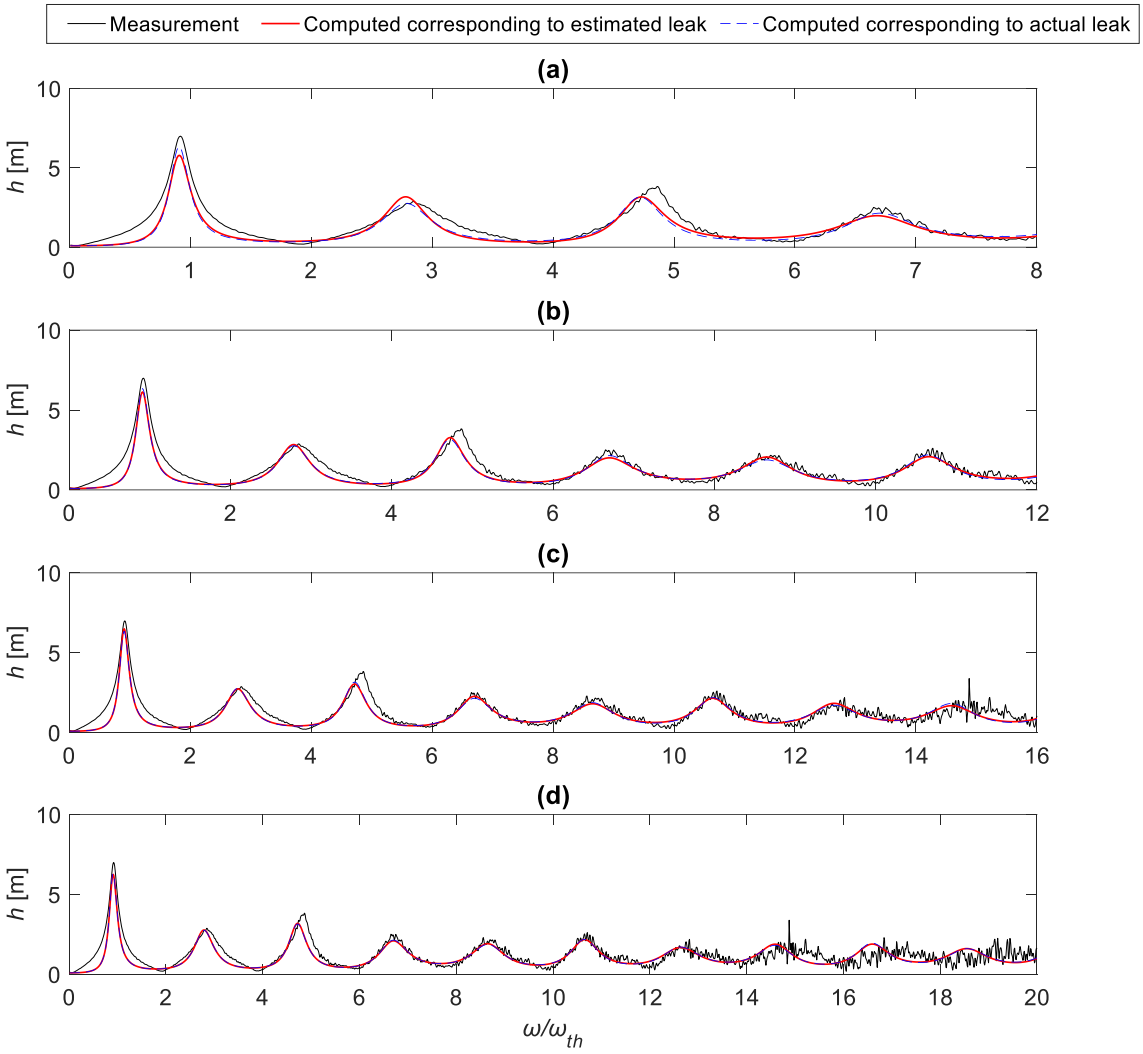

Fig 14 Reconstructed spectra corresponding to the estimated and actual leak (in continuous red and dashed blue, respectively) along with the original measurement (in continuous black) in Perugia experiment; (a)-(d) correspond to the localizations plotted in Fig. 13a-d, respectively, i.e. for different signal bandwidth $\omega = \omega_{th} \times (1{:}\,0.01{:}\,n_{\max})$, (a) $n_{\max} = 8$, (b) $n_{\max} = 12$, (c) $n_{\max} = 16$, (d) $n_{\max} = 20$.

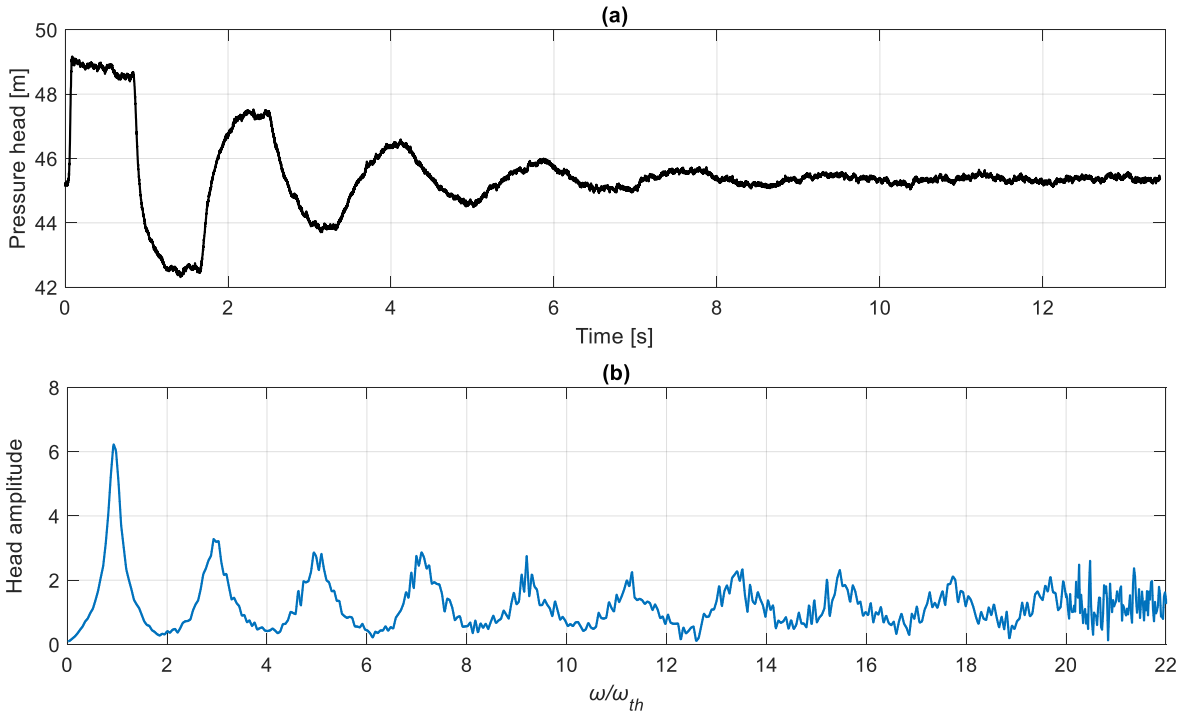

Fig 15 Measurements of pressure head at the downstream valve in the HKUST experiment; (a) time domain, and (b) frequency domain data.

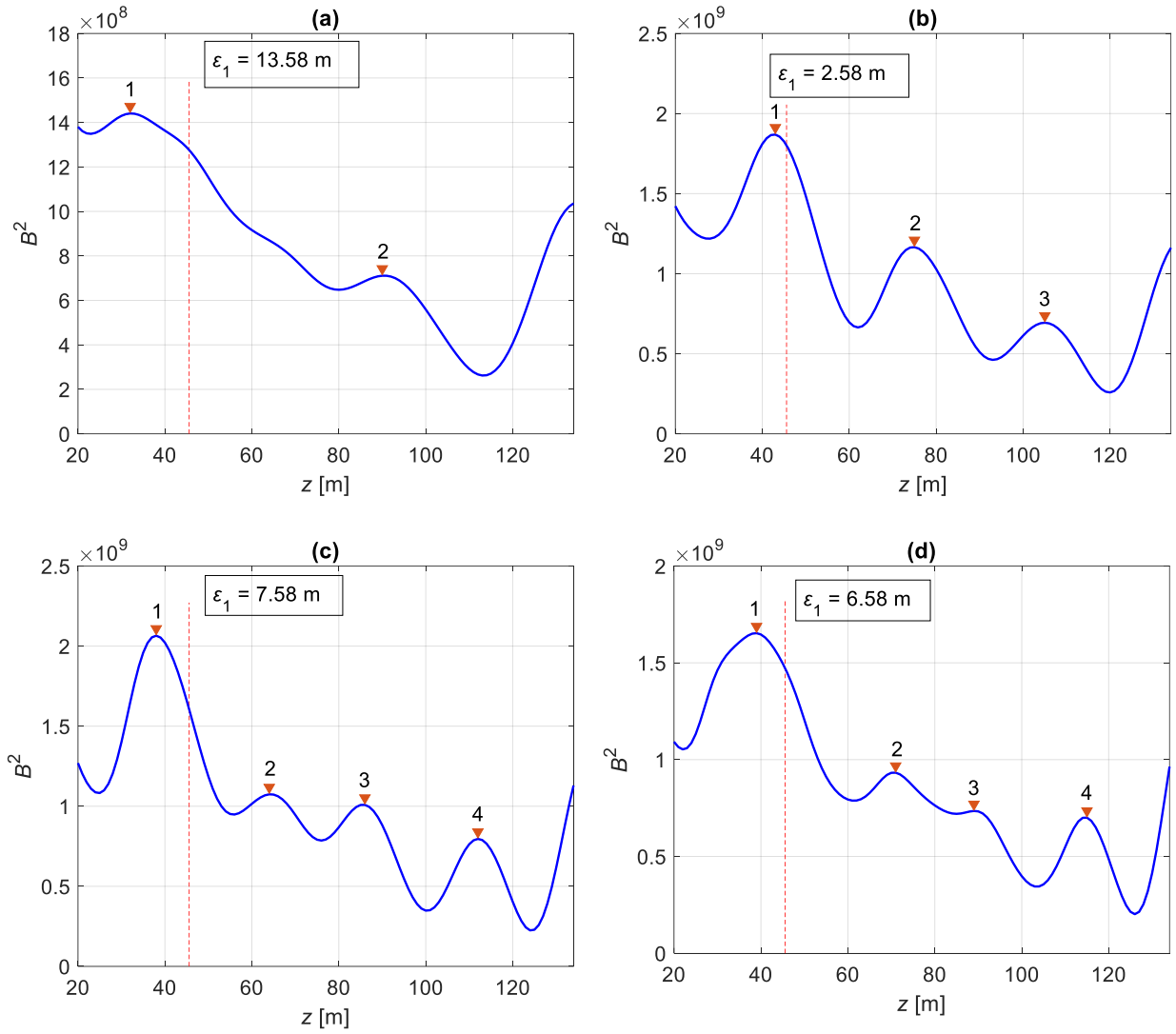
(a)
$\times 10^8$
ε_1 = 13.58 m
1
2
B^2
z [m]
(b)
$\times 10^9$
ε_1 = 2.58 m
1
2
3
B^2
z [m]
(c)
$\times 10^9$
ε_1 = 7.58 m
1
2
3
4
B^2
z [m]
(d)
$\times 10^9$
ε_1 = 6.58 m
1
2
3
4
B^2
z [m]

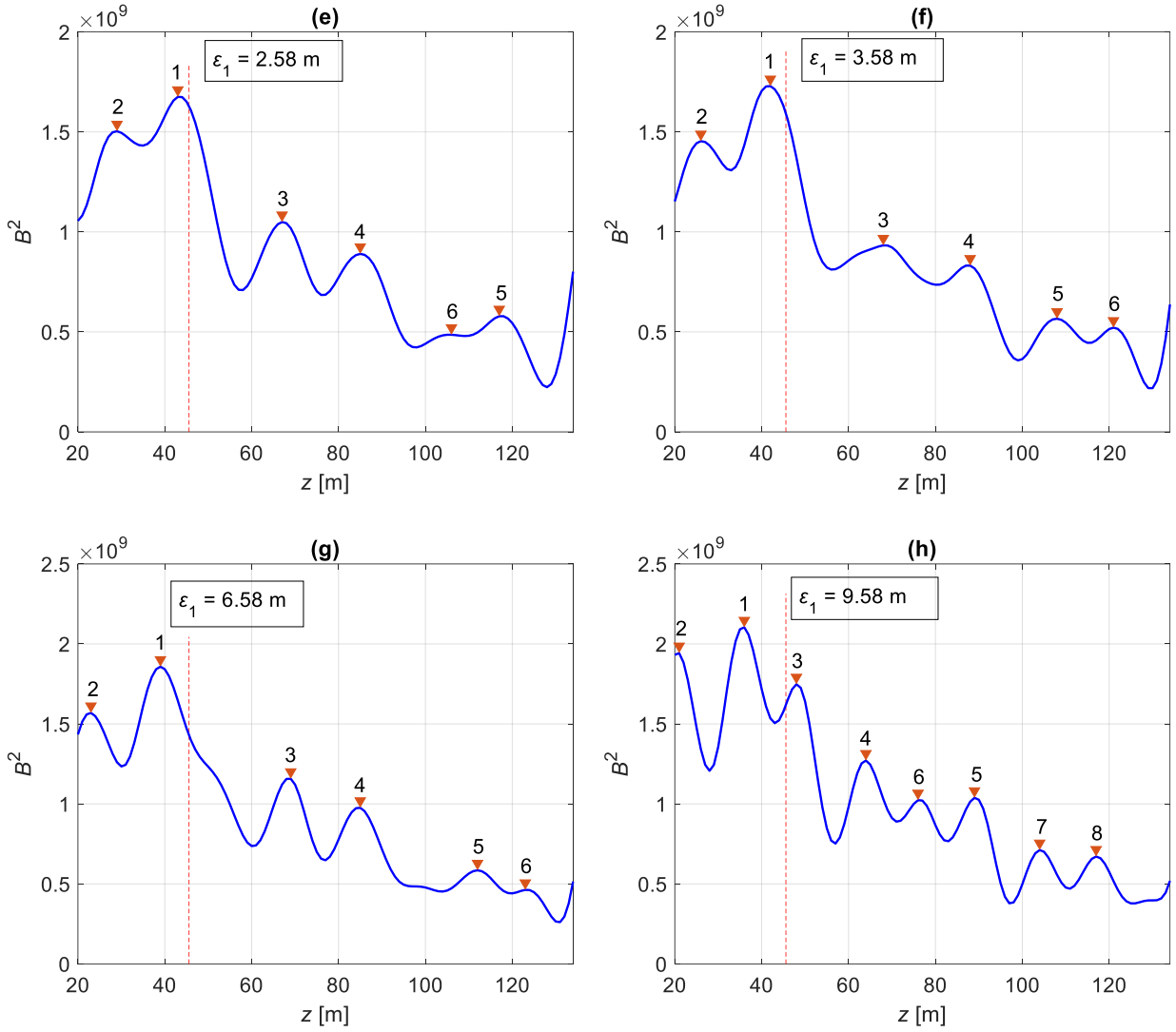

Fig 16 Localization results of the proposed method for the Hong Kong experiment when different signal bandwidth $\omega = \omega_{th} \times (1{:}\,0.01{:}\,n_{\max})$ is incorporated: (a) $n_{\max} = 8$, (b) $n_{\max} = 10$, (c) $n_{\max} = 12$, (d) $n_{\max} = 14$, (e) $n_{\max} = 16$, (f) $n_{\max} = 18$, (g) $n_{\max} = 20$, (h) $n_{\max} = 22$.

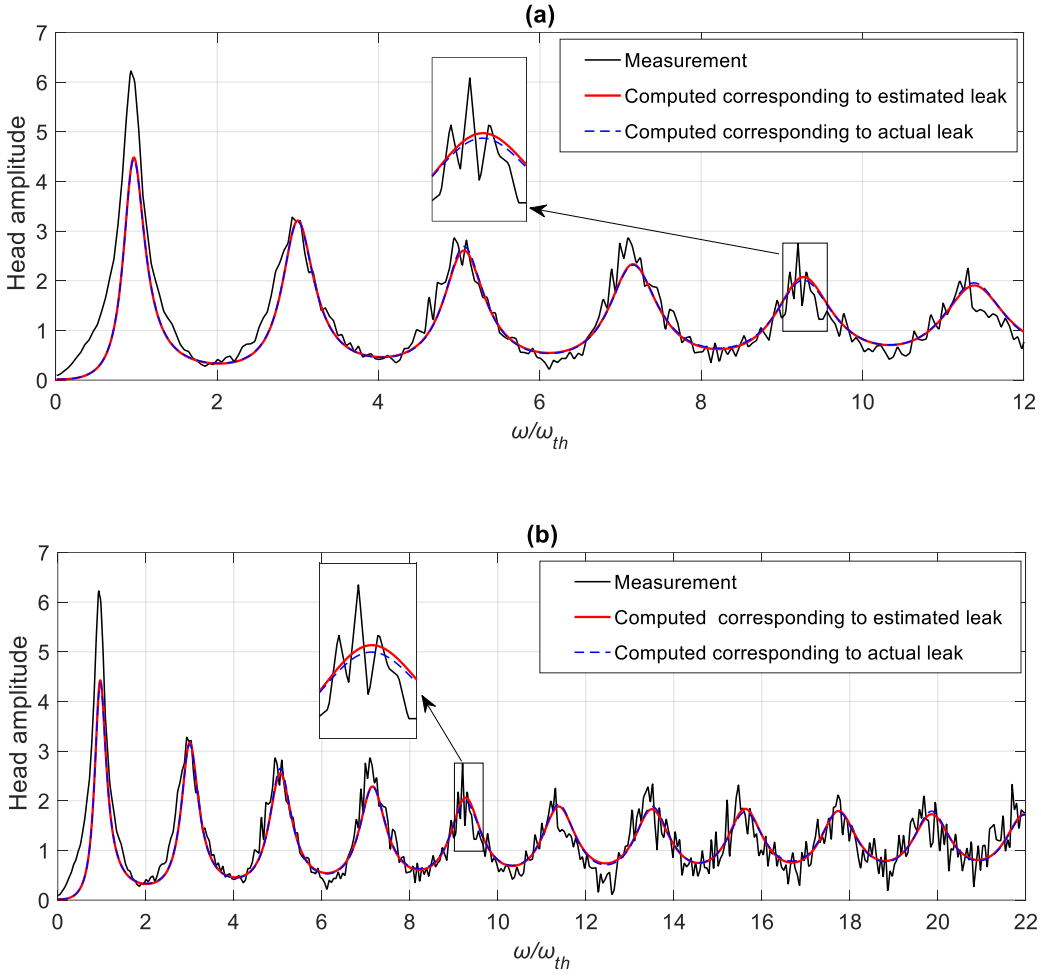

Fig 17 Reconstructed spectra corresponding to the estimated and actual leak (in continuous red and dashed blue, respectively) along with the original measurement (in continuous black) in HKUST test; (a)-(b) correspond to the localizations plotted in Fig. 16c with $n_{\max} = 12$, and Fig. 16h, with $n_{\max} = 22$, respectively.

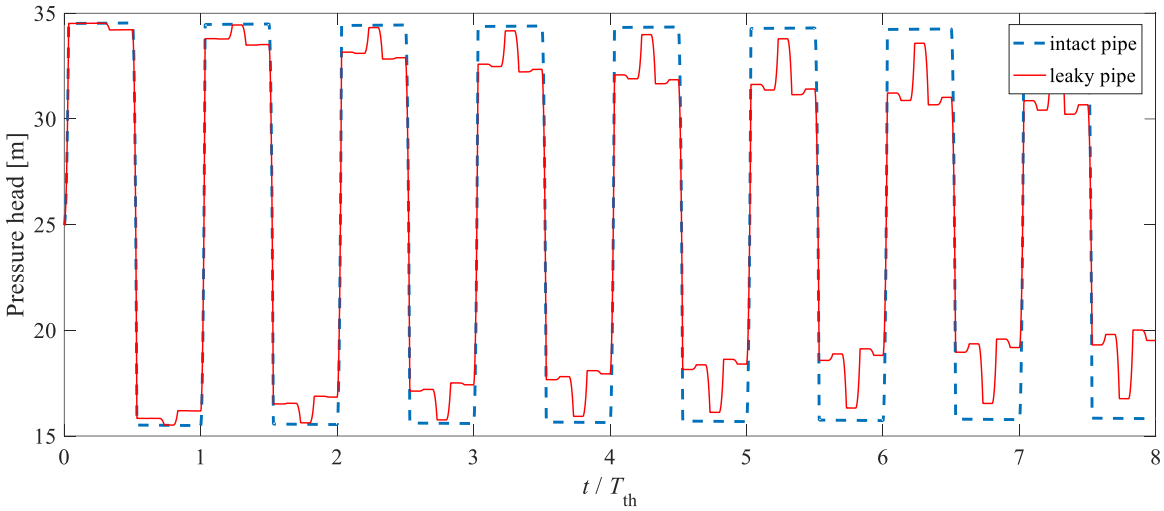

Fig 18 Pressure head in the time domain at the downstream valve to be considered as the measurement vector in the identification procedure.

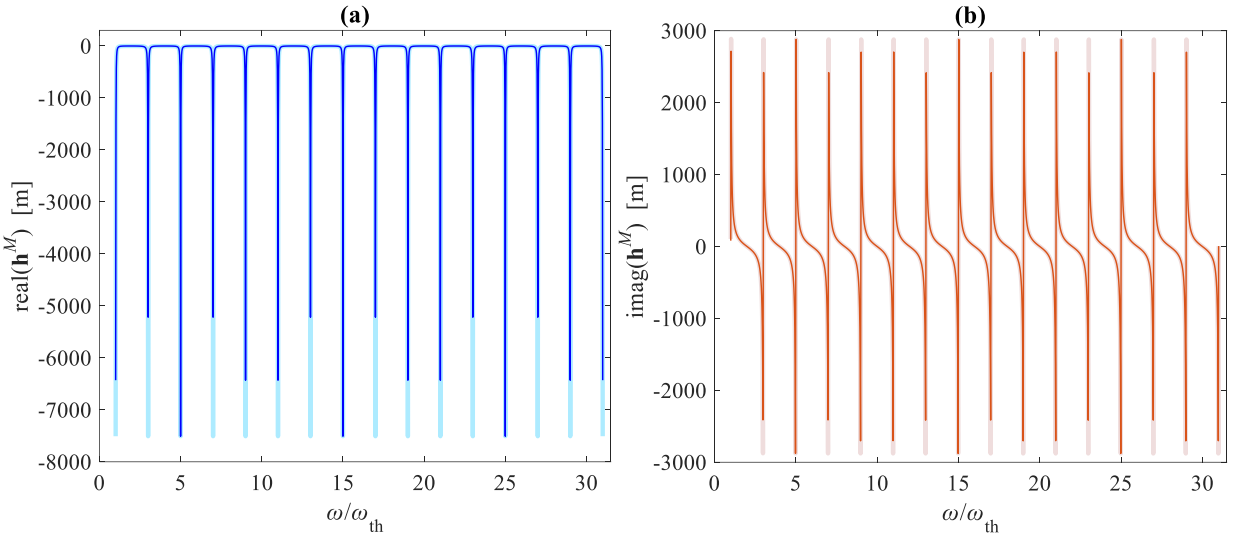

Fig 19 Real part (a, blue curve) and imaginary part (b, red curve) of the pressure head spectra at the valve position corresponding to the intact (light colour) and leaky pipe (dark colour).

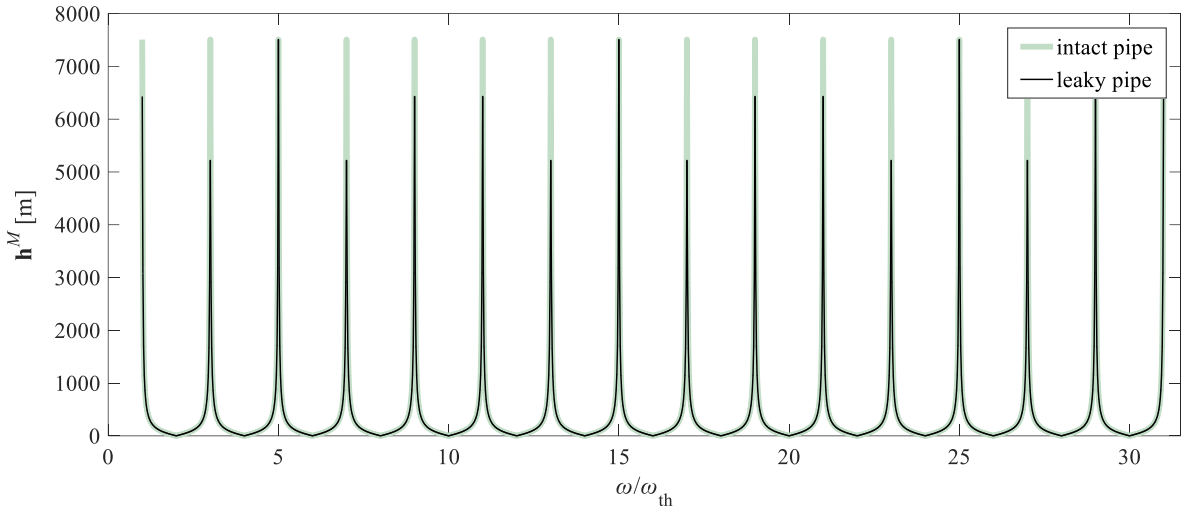

Fig 20 The amplitudes of the pressure head spectra corresponding to the intact pipe (in light green colour) and leaky pipe (in black).